Cyclic Peptoids as Mycotoxin Mimics: An Exploration of Their Structural and Biological Properties

Assunta D'Amato,[†] Raffaele Volpe,[†] Maria Carmela Vaccaro,[‡] Stefania Terracciano,[‡] Ines Bruno,[‡] Massimo Tosolini,[§] Consiglia Tedesco,[†] Giovanni Pierri,[†] Paolo Tecilla,[§] Chiara Costabile,[†] Giorgio Della Sala,[†] Irene Izzo,*[,†] and Francesco De Riccardis*[,†]

[†]Department of Chemistry and Biology "A. Zambelli" and [‡]Department of Pharmacy, University of Salerno, Via Giovanni Paolo II, 132, Fisciano (SA) 84084, Italy

[§]Department of Chemical and Pharmaceutical Sciences, University of Trieste, Via Giorgieri, 1, Trieste 34127, Italy

Supporting Information

ABSTRACT: Cyclic peptoids have recently emerged as important examples of peptidomimetics for their interesting complexing properties and innate ability to permeate biological barriers. In the present contribution, experimental and theoretical data evidence the intricate conformational and stereochemical properties of five novel hexameric peptoids decorated with *N*-isopropyl, *N*-isobutyl, and *N*-benzyl substituents. Complexation studies by NMR, in the presence of sodium tetrakis[3,5-bis(trifluoromethyl)phenyl]borate (NaTFPB), theoretical calculations, and single-crystal X-ray analyses indicate that the conformationally stable host/guest metal adducts display architectural ordering comparable to that of the enniatins and beauvericin mycotoxins. Similarly to the natural depsipeptides, the synthetic oligolactam analogues show a correlation between ion transport abilities in artificial liposomes and cytotoxic activity on human cancer cell lines. The reported results demonstrate that the versatile cyclic peptoid scaffold, for its remarkable conformational and complexing properties, can morphologically mimic related natural products and elicit powerful biological activities.

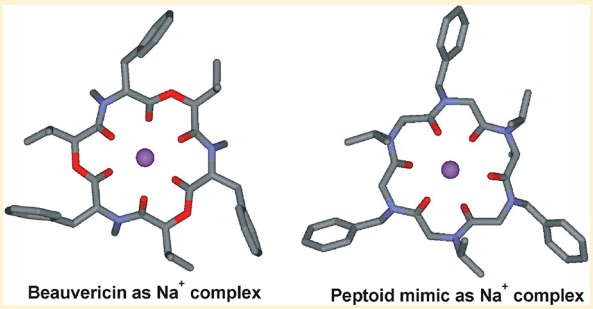

INTRODUCTION

In the last four billion years, molecular evolution has created an astounding archive of secondary metabolites.[1] The conspicuous diversity of this extraordinary library of chemical entities has prompted organic and medicinal chemists to decipher structures, assess therapeutic potential, and design simpler artificial mimics, shifting the supply of bioactive molecules from Nature to imagination.[2]

In our long journey through the fecund territory of peptoids (oligomers of N-substituted glycines),[3] we tried to grasp how the cyclic peptoid morphology relates to function[4] and learned how to generate Nature's inspired molecular architectures from minimal building blocks.[5]

In this contribution, we demonstrate that an assembly of properly chosen achiral *N*-alkyl glycines, once oligomerized and cyclized, can mimic the class of bioactive fungal cyclo-oligomer depsipetides enniatins and beauvericin[6] (Figure 1) and exert powerful cytotoxic activity on cancer cell lines. For their structural properties and conformational stability, the N-substituted cyclic peptoids can evoke the occurrence of a nonclassical type of chirality[7] and, once mixed with proper amounts of sodium cation, give rise to complexes of magnificent beauty and remarkable symmetry in both solid state and solution.

Enniatins and beauvericin are cyclic depsipeptides (hybrid structures composed of α-amino acids and α-hydroxyacids), showing a broad spectrum of anticancer, antihelmintic, antibiotic, antifungal, insecticidal, hypolipidaemic, and antiretroviral activities.[6b−e,8] The reported enniatins **1**−**7** (Figure 1) were selected among the 29 so far isolated (mainly from fungi belonging to the *Fusarium* genus).[6c] Beauvericin (**8**), first isolated from the fungus *Beauveria bassiana*, differs from the enniatins for the presence of aromatic side chains.[6d]

Owing to the steric strain caused by the α-branched *N*-methyl-(*S*)-amino acids[9] (commonly, *N*-methylvaline and *N*-methyl-isoleucine; R_1, R_2, and R_3 residues, Figure 1) and to the bulky (*R*)-hydroxyisovaleric acid (Hiv; R_4 residue), enniatins and beauvericin are conformationally stable and show sharp signals in the NMR spectra.[10] Their pore shape[11] confirms the well-known ionophoric behavior[12] and the broad range of biological activities.[6,8,10a]

In order to better understand the architectural determinants of the enniatins/beauvericin class and with the idea to explore the latent properties withheld by the cyclic peptoids scaffold, we designed **9**, **10**, and **11** as structural mimics of enniatin B (enB), enniatin C (enC), and beauvericin (bv), respectively (Figure 2). Analogues **12**, **13**, and the known[13] **14**, although not isomorph

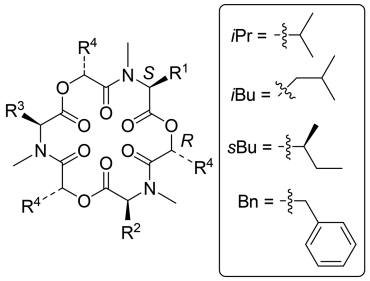

Mycotoxin	R^1	R^2	R^3	R^4
Enniatin A (**1**)	*s*Bu	*s*Bu	*s*Bu	*i*Pr
Enniatin B (**2**, enB)	*i*Pr	*i*Pr	*i*Pr	*i*Pr
Enniatin C (**3**, enC)	*i*Bu	*i*Bu	*i*Bu	*i*Pr
Enniatin D (**4**)	*i*Pr	*i*Pr	*i*Bu	*i*Pr
Enniatin E_1 (**5**)	*i*Pr	*i*Bu	*s*Bu	*i*Pr
Enniatin F (**6**)	*i*Bu	*s*Bu	*s*Bu	*i*Pr
Enniatin G (**7**)	*i*Bu	*i*Bu	*i*Pr	*i*Pr
Beauvericin (**8**, bv)	Bn	Bn	Bn	*i*Pr

Figure 1. Representative natural cyclohexadepsipeptide mycotoxins enniatins and beauvericin.

with natural enniatins/beauvericin, were included in the study in order to enlarge the scope of the investigation.

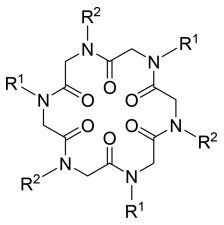

Cyclic peptoid	R^1	R^2
9 (enB)	*i*Pr	*i*Pr
10 (enC)	*i*Bu	*i*Pr
11 (bv)	Bn	*i*Pr
12	*i*Bu	*i*Bu
13	Bn	*i*Bu
14	Bn	Bn

Figure 2. Structures of the new cyclic peptoids **9**−**13** and the known **14** included in the present study. In parentheses are reported the natural counterparts.

The conversion of the depsipeptide frame in a lactam core[14] preserves the relative positions of carbonyl groups/side chains[15] (Figures 1 and 2) but has the effect to weaken the conformational stability. Spectroscopic, theoretical, and single-crystal X-ray diffraction analyses herein reported demonstrate that the coordinating ability of Na^+ ion,[4b,d,e] restores the conformational stability of cyclic peptoids **9**−**14** promoting potent ionophoric[16] and cytotoxic activity.[17,3g]

RESULTS AND DISCUSSION

Synthesis and Structural Studies. The manual solid-phase synthesis proceeded smoothly for each of the five new linear precursor peptoids **15**−**19** (Figure 3). The classic "submonomer" protocol[18] was performed on the 2-chlorotrityl solid support (a sterically congested resin that drastically reduces the diketopiperazine formation). The couplings were monitored after the amidation step (performed in the presence of bromoacetic acid and DIC as the condensing agent) and invariably gave negative chloranil tests. The oligomers were detached from the resin using the slightly acidic 1,1,1,3,3,3-hexafluoro-2-propanol (HFIP). The crude linear peptoids were cyclized under high dilution conditions (3.0×10^{-3} M) in the presence of HATU[19] as the condensing agent and yielded the cyclic hexameric peptoids **9**−**13** (Figure 2) in high purity (>95%, HPLC analysis; see Supporting Information) through precipitation from hot acetonitrile or reverse-phase chromatographic purification and acceptable yields (36−65%; see Experimental Section).

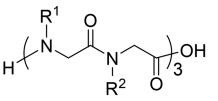

Oligomer	R^1	R^2	Sequence	Yield
15	*i*Pr	*i*Pr	H-[*N*Val]$_6$-OH	100%
16	*i*Bu	*i*Pr	H-[*N*Leu-*N*Val]$_3$-OH	92%
17	Bn	*i*Pr	H-[*N*Phe-*N*Val]$_3$-OH	87%
18	*i*Bu	*i*Bu	H-[*N*Leu]$_6$-OH	76%
19	Bn	*i*Bu	H-[*N*Phe-*N*Leu]$_3$-OH	78%

Figure 3. Solid-phase synthesis of linear peptoids **15**−**19**: sequences and chemical yields.

The ^{1}H NMR spectra recorded for the mycotoxin congeners **9**−**14** ($CDCl_3$, Figure 4) evidenced diversified conformational stability. In the case of the enB analogue **9**, the relatively bulky

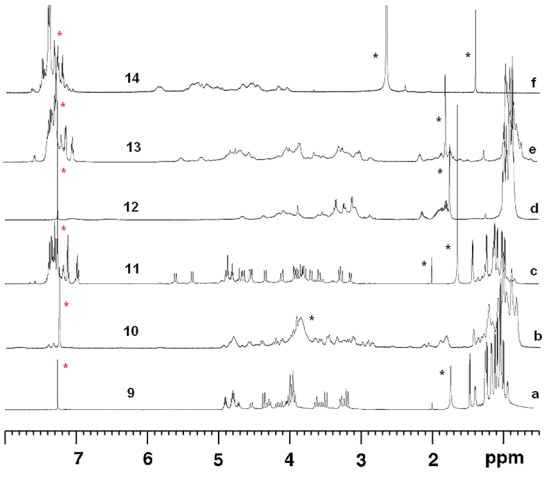

Figure 4. ^{1}H NMR spectra of cyclic peptoids **9**−**14**. Residual solvent peaks are labeled with a red asterisk. Impurities (mainly water) are labeled with a black asterisk; 5.0−10.0 mM solutions in $CDCl_3$ (600 MHz).

isopropyl groups stiffen the 18-membered ring, giving multiple discernible conformers (Figure 4a). The ^{1}H NMR spectra of compounds **10** and **12**–**14** (with α-branched *N*-isobutyl and *N*-benzyl groups) show broad signals, indicating equilibrium between two or more conformations in slow exchange on the NMR time scale (Figure 4b,d–f). Surprisingly, the ^{1}H NMR spectrum of the alternated *N*-isopropyl/*N*-benzyl beauvericin congener **11** showed the presence of a major conformational isomer (~85%, Figure 4c).[20] The 2D homonuclear (COSY) and heteronuclear (HMQC, HMBC) experiments allowed full assignment of the ^{1}H/^{13}C resonances.[21] The *cis*/*trans* peptoid bond junctions of the *N*Val residues were assigned on the basis of the ^{1}H NMR *N*-Cα*H* chemical shift values, as previously reported for the case of (*S*)-phenylethyl side chains.[22] In particular, higher chemical shift values (δ 4.87 and 4.78 ppm) indicated *cis* amide bond geometries (side chains *syn* to the deshielding carbonyl groups); a lower chemical shift value (δ 3.81 ppm) implied a *trans* amide geometry. In the case of the benzyl groups, the amide bond geometries were deduced by the $\Delta\delta$ values of the diastereotopic *N*–CH_2–Ph protons. A marked difference in their values ($\Delta\delta$ = 1.82 and 1.59 ppm) suggested the presence of a *cis* peptoid bond (*syn* relationship with the carbonyl group), a small $\Delta\delta$ (0.19 ppm) pointed toward a *trans* peptoid bond.

The presence of interfering ROE cross-correlations (see Supporting Information) belonging to the unidentified minor conformational isomers hampered the residues' sequence assignment. Instructive long-range ^{1}H/^{13}C connectivities (Figure 5) inferred a cyclo-[*cis*-*N*Val^1-*cis*-*N*Phe^1-*trans*-*N*Val^2-*cis*-*N*Phe^2-*cis*-*N*Val^3-*trans*-*N*Phe^3] (i.e., cyclo-[*cctcct*])[23] arrangement for the conformationally stable[24] **11** (see Table 1 for full NMR data and assignments).

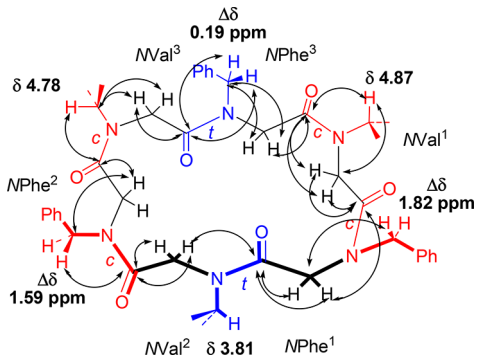

Figure 5. (a) Schematic solution structure of cyclo-[*cctcct*]-**11** and relevant long-range ^{1}H–^{13}C cross-correlations (from HMBC).

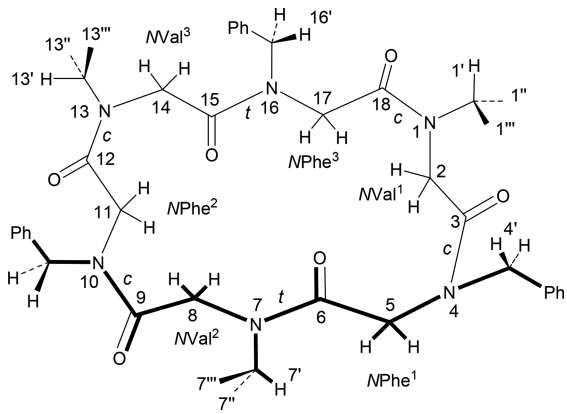

Further support for the cyclo-(*cctcct*) arrangement came from comparison of the relative stability of the conformations, as judged from the internal energies differences (ΔE) calculated in $CHCl_3$, among cyclo-[*cctcct*]-**11** and the two possible alternative diastereomeric *cis*/*trans* isomers: cyclo-[*cis*-*N*Val-*cis*-*N*Phe-*trans*-*N*Val-*trans*-*N*Phe-*cis*-*N*Val-*cis*-*N*Phe]-**11a** and cyclo-[*cis*-*N*Phe-*cis*-*N*Val-*trans*-*N*Phe-*trans*-*N*Val-*cis*-*N*Phe-*cis*-*N*Val]-**11b** (see Supporting Information for structures and computational details). The calculated values increased in the order: **11** (E = 0 kJ mol^{-1}) < **11b** (ΔE = 48.6 kJ mol^{-1}) < **11a** (ΔE = 71.9 kJ mol^{-1}), thus confirming the ^{1}H NMR results.

In addition to the collected data, we were also able to obtain single crystals suitable for X-ray diffraction analysis for compounds **9** (by slow evaporation from a solution of 1:1 chloroform/methanol) and **11** (by slow diffusion of hexane vapors in a chloroform solution).

As expected, the X-ray molecular structure of compounds **9** and **11** showed a *cctcct* amide bond sequence (Figures 6 and 7), in accordance to all the other metal-free hexameric cyclic peptoids previously studied by X-ray diffraction.[23]

Similarly to cyclo-$(Sar)_6$[25] and cyclo-$(Npm\text{-}Nme)_3$,[26] the side groups point alternatively in opposite directions with respect to the plane defined by the peptoid backbone. In compound **11**, the isopropyl and benzyl side chains are clustered on opposite sides of the macrocycle, as shown in Figure 7b.

Compound **9**, obtained as a solvent-free form, constitutes ribbons along the shortest cell axis (*a* axis) by means of side-by-side CO···H_2C hydrogen bonds involving carbonyl oxygen atoms and backbone methylene hydrogen atoms. Compound **11** crystallizes as a chloroform solvate with a 1:2 ratio between cyclopeptoid and chloroform molecules. Cyclopeptoid molecules form ribbons parallel to the diagonal of the *ac* plane by means of side-by-side CO···HC hydrogen bonds involving carbonyl oxygen atoms and side chain methylene hydrogen atoms of the *trans* residues. The side-by-side assembly always involves the same type of *trans* residue (e.g., *i*-Pr side chains are alongside *i*-Pr side chains, and benzyl side chains are alongside benzyl side chains).

Both crystallographically independent chloroform molecules interact with carbonyl oxygen atoms by CH···O hydrogen bonds. It is worth noting that the beauvericin crystal structure corresponds to a hydrate form, with the cyclodepsipeptide featuring all side chains in a pseudoequatorial position[27]

The structural comparison between the minimum energy conformation predicted for beauvericin analogue cyclo-[*cctcct*]-**11** (with a backbone almost superimposable to the solid state structure reported in Figure 7a) and the pore-shaped beauvericin **8** (inferred from theoretical studies)[11c,28] showed an evident morphological diversity of the two species (Figure 8). It is known, however, that the conformational attitudes of peptoids change dramatically in the presence of metal cations.[29] We, thus, modeled [**11**·Na]$^+$ on the basis of the all-*trans* geometry arrangement found for the cyclic hexameric peptoids metal complexes.[4b,e,19,23] Figure 8c shows the similarity between [**11**·Na]$^+$ and beauvericin (**8**): this time in both compounds the side chain orientation and back-bone morphologies are clearly comparable.

Conformational Chirality. There is another, more subtle, qualitative peculiarity linking some metalated cyclic peptoids and the natural cyclodepsipeptides: their chirality. Despite the lack of stereogenic centers, axes, and planes of chirality,[7] the presence of directional bonds in conformationally rigid[30] cyclic structures can induce a chiral arrangement. In this context, the theoretical

Table 1. ^{1}H and ^{13}C NMR Chemical Shifts for Cyclic Peptoid 11[a]

C/H number	C	H	*N*-Aa
1′	44.8	4.87 (1H, d, *J* 7 Hz)	*cis*-*N*Val$_1$
1″	20.2	1.08 (3H, d, *J* 7 Hz)	
1‴	19.6	1.13 (3H, d, *J* 7 Hz)	
2	44.2	4.53, 3.70 (2H, d, *J* 17 Hz)	
3	169.9		
4′	51.3	5.60, 3.78 (2H, d, *J* 15 Hz)	*cis*-*N*Phe$_1$
5	47.6	4.11, 3.92 (2H, d, *J* 17 Hz)	
6	167.1		
Ar	136.2[b]	7.40−7.25 (5H, overlapping signals)	
	128.8		
	128.4		
	127.6		
7′	48.0	3.81 (1H, d, *J* 7 Hz)	*trans*-*N*Val$_2$
7″	21.5	1.41 (3H, d, *J* 7 Hz)	
7‴	21.2	1.23 (3H, d, *J* 7 Hz)	
8	42.7	4.34, 3.29 (2H, d, *J* 17 Hz)	
9	171.9		
10′	51.9	5.37, 3.90 (2H, d, *J* 15 Hz)	*cis*-*N*Phe$_2$
11	50.8	4.67, 3.27 (2H, d, *J* 17 Hz)	
12	168.8		
Ar	137.3[b]	7.40−7.25 (5H, overlapping signals)	
	128.8		
	127.7		
	127.6		
13′	45.7	4.78 (1H, d, *J* 7 Hz)	*cis*-*N*Val$_3$
13″	20.4	0.98 (3H, d, *J* 7 Hz)	
13‴	19.5	1.01 (3H, d, *J* 7 Hz)	
14	43.2	3.85, 3.59 (2H, d, *J* 17 Hz)	
15	168.7		
16′	53.1	4.90, 4.71 (2H, d, *J* 15 Hz)	*trans*-*N*Phe$_3$
17	50.3	4.54, 3.14 (2H, d, *J* 17 Hz)	
18	170.9		
Ar	135.5[b]	6.98 (2H, t, *J* 7.5 Hz, Ar-*m*-*H*), 7.40−7.25 (3H, overlapping signals)	
	129.1		
	127.5		
	125.6		

[a]Assignment based on COSY, HSQC, and HMBC experiments (^{1}H at 600 MHz, ^{13}C at 150 MHz, $CDCl_3$, major isomer; see Supporting Information). [b]Phenyl quaternary carbon.

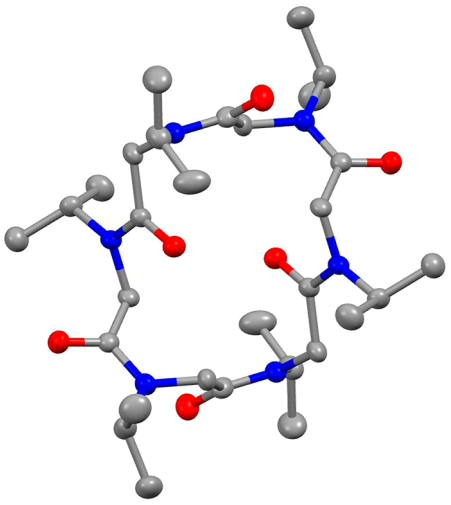

Figure 6. X-ray molecular structure of the cyclic peptoid enB mimic **9**. Hydrogen atoms have been omitted for clarity. Atom type: C, gray; N, blue; O, red. Thermal ellipsoids are drawn at 30% probability level.

model for the all-*trans*-[**11**·Na]$^+$ complex, reported in Figure 8b, is instructive. A closer look to its schematic structure (Figure 9a, reporting the out-of-plane amide bonds) demonstrates that this complex is chiral and that the two enantiomers (Figure 9a,b) can also be derived by ring inversion (Figure 9c).

The same holds true also for the conformationally stable[24] free host cyclo-[*cctcct*]-**11**, which is present in two enantiomeric forms (**11a** and **11c**; see Figure S37 in the Supporting Information). Proof of its chirality is the clear 1:1 splitting of some ^{1}H NMR resonances induced by the gradual addition of the chiral solvating agent Pirkle's alcohol ((*R*)-1-(9-anthryl)-2,2,2-trifluoroethanol, as reported in Figures S38 and S39 of the Supporting Information). Another clear evidence of its chirality comes from the diffractometric data: both the enantiomers (**11a** and **11c**) are present in the crystal packing (see Figure S36 in the Supporting Information).

A chirality of noncovalent origin due to long-average time of bonds rotation is defined as "conformational chirality"[7a,b] ("conformational cycloenantiomerism",[31] "inherent chirality",[32] and "cyclochirality"[33,34] refer to conceptually different cases).

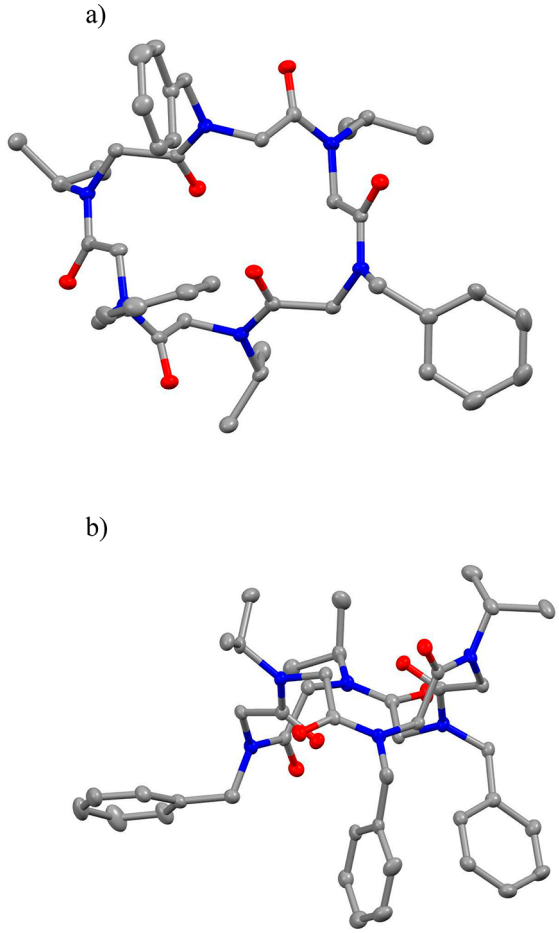

Figure 7. X-ray molecular structure of the cyclic peptoid beauvericin mimic **11**, top view (a) and side view (b). Hydrogen atoms have been omitted for clarity. Atom type: C, gray; N, blue; O, red. Thermal ellipsoids are drawn at 30% probability level.

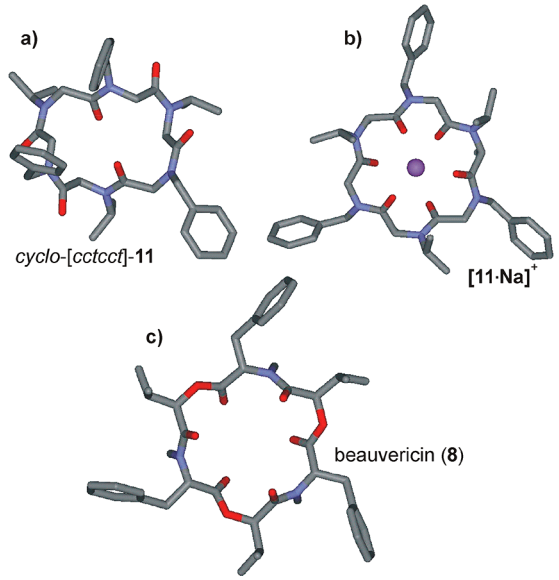

Figure 8. Comparison among theoretically calculated solution structures of cyclo-[*cctcct*]-**11** (a), all-*trans*-[**11**·Na]$^+$ complex (b), and beauvericin (**8**, c). Hydrogen atoms have been omitted for clarity. Atom type: C, gray; N, light blue; O, red; Na$^+$, magenta.

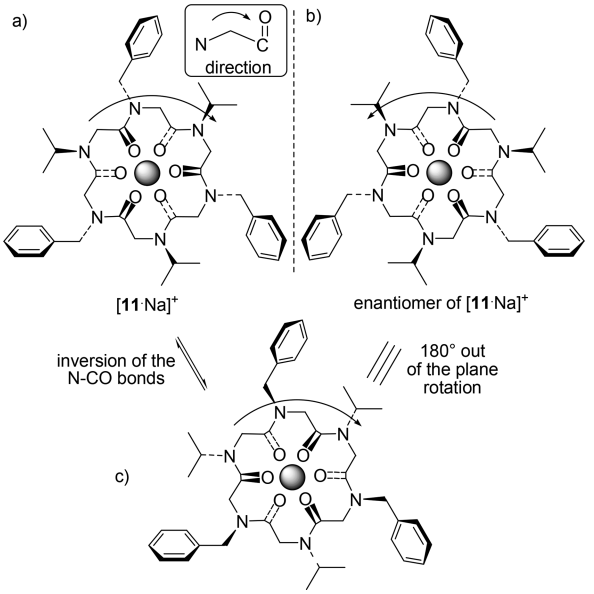

Figure 9. Schematic structure of (a) [**11**·Na]$^+$, (b) its mirror image, and (c) conformational isomer of [**11**·Na]$^+$, coincident with its mirror image. Hexacoordinated Na$^+$ ion is represented by the gray sphere. Amide bonds are considered as ideal planes.

It is worth noting that the possible formation of enantiomers in the case of the sodium complexes of cyclic peptoids **10**, **11**, and **13**[35] should not be detrimental to the biological activities. It is known, in fact, that both the enantiomers of enniatin A and B are equally bioactive[36] as their target is the cellular membrane (which is not a chiroselective receptor).[36,37]

The experimental assessment of the sodium complexing abilities for the cyclopeptoid array **9**–**14** was thus considered a necessary step to fully disclose the structural and biological potential of the designed molecules.

Sodium Binding Studies. Sodium binding[38] studies were performed in the presence of sodium tetrakis[3,5-bis-(trifluoromethyl)phenyl]borate (NaTFPB)[39,4a] and investigated by ^{1}H NMR in $CDCl_3$. NaTFPB promotes tight metal binding for the intrinsic coordinating weakness of the TFPB counterion. The formation of symmetric metalated species and the negligible solubility of the free guest in nonpolar solvents reveals the complex stoichiometry by simple ^{1}H NMR host/guest signals integration.[4a]Preliminary quantitative experiments, upon addition of 1.0 equiv of NaTFPB, confirmed metal binding for all the cyclic peptoids (Figure 10).

The low chemical shift values observed for the *N*Val Cα*H* residues (4.06 ppm in [**9**·Na]$^+$, 3.98 ppm in [**10**·Na]$^+$, 3.89 ppm in [**11**·Na]$^+$), the relatively small $\Delta\delta$ evidenced for the diastereotopic *N*–CH_2–Ph protons (0.49 ppm in [**11**·Na]$^+$, 0.41 in [**13**·Na]$^+$, 0.30 in [**14**·Na]$^+$), and the support of literature data[4b,d,e,19,40] suggested, for all the conformers, all-*trans* amide bonds geometries. The strong electrostatic forces between the sodium ion and the carbonyl dipoles stabilize the metalated conformers, hampering the ring inversion (with no sign of diastereotopic protons' signals coalescence) up to 393 K for the six [**9**–**14**·Na]$^+$ complexes (^{1}H NMR variable temperature experiments: 1.0 mM solutions in $C_2D_2Cl_4$, 600 MHz).

^{1}H NMR spectra of NaTFPB stepwise quantitative additions showed, for all the analyzed peptoids, gradual formation of symmetric metalated species at the expense of the multiple conformations of the free hosts. The integration value *ratios*

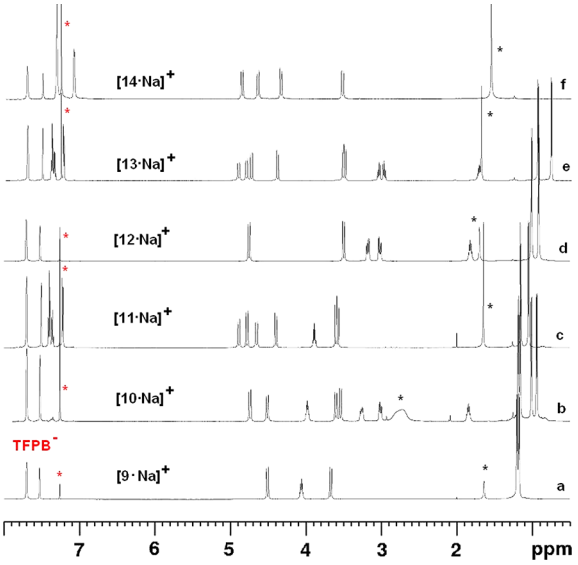

Figure 10. ^{1}H NMR spectra showing the metal binding of cyclic peptoids **9**−**14** in the presence of 1.0 equiv of NaTFPB. Residual solvent peaks are labeled with a red asterisk. Water impurities are labeled with a black asterisk; 5.0−10.0 mM host/guest solutions in $CDCl_3$ (600 MHz).

between the symmetric host/guest complexes and the TFPB aromatic resonances were constant during the titrations and documented a fixed 1:1 macrocycle/Na^+ ratio for all the complexes. Further proof of the 1:1 host/guest stoichiometry was deduced by the plots reporting the declining percentage of the free hosts (calculated on the basis of the 2.5−6.0 ppm range integration) versus the molar Na^+/cyclopeptoid ratio.

The graphs showed absence of free host after reaching a 1:1 stoichiometry. Figure 11 reports the exemplary case recorded for

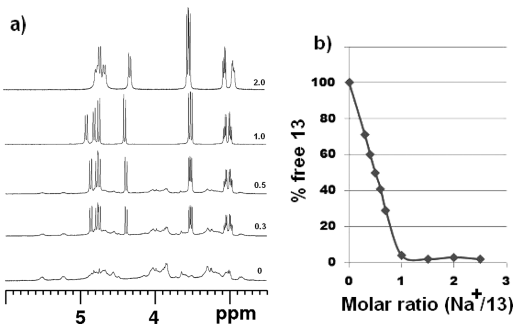

Figure 11. ^{1}H NMR quantitative titration of **13** with NaTFPB at the molar ratio indicated (a) and plot (b) reporting the percentage of **13** as free host versus the molar ratio Na^+/**13**. The data were extrapolated by spectra recorded in $CDCl_3$ at 25 °C (5.0 mM peptoid concentration, 600 MHz).

the most soluble host **13** (similar trends were observed for **9**−**12** and **14**). Addition of NaTFPB beyond 1.0 equiv induced variation of the chemical shift values, witnessing the possible formation of a further metalated species (see difference in the chemical shift between the two top spectra in Figure 11a).

Table 2 reports the calculated apparent association constants (as log K_{a1}) values[4a,41] and the corresponding Gibbs free energy values for the formation of the [**9**−**14**·Na]$^+$ complexes (calculated by ^{1}H NMR, 1.0 mM in $CDCl_3$). The results show lower sodium affinities for the cyclic peptoids with isopropyl side

Table 2. Calculated Apparent[41b,c] K_{a1} (M^{-1}) Values and $-\Delta G°$ (kcal/mol) for the [9−14·Na]$^+$ Complexes

	9	10	11	12	13	14
log K_{a1}[a,b]	3.2	4.2	4.0	4.9	4.8	4.9
$-\Delta G°$	4.4	5. 8	5.5	6.6	6.5	6.6

[a]from ^{1}H NMR experiments, 1.0 mM host/guest in $CDCl_3$ solutions. [b]Figures within ±10% throughout multiple experiments.

chains (the lowest value associated with **9**—enB analogue—with six isopropyl groups).

Metal binding studies conducted on enniatins/beauvericin (by ^{1}H NMR, CD, ORD, and molecular modeling)[10a] showed variegated macrocycle/metal stoichiometric ratios (1:1, 2:1, 3:1) depending on metal cations' size and solvents' dielectric constant. In our case, sodium titration studies indicated no macrocycle/metal complexing stoichiometry ratios higher than one. Interestingly, further addition of NaTFPB to [**9**−**14**·Na]$^+$ led to the formation of rare O-bound 1:2 macrocycle/cation [**10**−**14**·2Na]$^{2+}$ complexes (no variations were recorded in the case of [**9**·Na]$^+$), which are defined as "inverse sandwich"[42] complexes.

The generation of the "inverse sandwich" complexes was demonstrated by the dissolution of a second equivalent of NaTFPB (testified by ^{1}H NMR signals' integration), by the shift of the ^{1}H NMR resonance values, with respect to the 1:1 complex, upon guest addition (implying a fast exchange, on the NMR time scale, of the second sodium ion with the monometal adduct), and by the electrospray spectra (formation of double charged species was observed; see Supporting Information).

For the $CDCl_3$ soluble complex [**13**·2Na]$^{2+}$, we were able to deduce the apparent[41b,c] K_{a2} value (^{1}H NMR, 1.0 mM in, using the program winEQNMR; see Figure S7, Supporting Information) by [**13**·Na]$^+$ complex titration with NaTFPB. The calculated apparent K_{a2} value was 52 M^{-1} (±10%). Unfortunately, partial precipitation of the [**10**−**12**,**14**·2Na]$^{2+}$ complexes in $CDCl_3$ hampered the evaluation of their apparent second association constant.[43]

According to density functional theory (DFT) studies, the formation of the bis-metalated species [**13**·2Na]$^{2+}$ would be favored with respect to the monometallic one [**13**·Na]$^+$. Indeed, the ΔG values for the formation of [**13**·Na]$^+$ and [**13**·2Na]$^{2+}$, in $CHCl_3$, starting from **13** and free Na^+ in solution were calculated to be −74.6 and −82.3 kJ mol^{-1}, respectively. The ΔG values for the formation of [**13**·Na]$^+$ and [**13**·2Na]$^{2+}$, in $CHCl_3$, starting from **13** and NaTFPB, were calculated to be −137.6 and −208.4 kJ mol^{-1}, respectively, showing that the formation of [**13**·2Na]$^{2+}$ would be favored if we assume the presence of free Na^+ in solution or if we consider the undissociated ionic couple.

[**13**·Na]$^+$ and [**13**·2Na]$^{2+}$ minimum energy structures are reported in Figure 12 (see Supporting Information for computational details).

It is interesting to note that, while in the 1:1 complex the cation is located inside the macrocycle cavity (Figure 12a, as also found in the X-ray structure of a triple decker Na^+ complex of symmetric prolinated peptoids),[4b] in the case of the "inverse sandwich" complex (Figure 12b), the two Na^+ ions share half of the amide carbonyl coordination sphere. Experimentally, we first observed the formation of the monosodium salts (as clarified by the representative plot reported in Figure 11 for **13**). Then, further addition of guest induced the formation of the disodium complexes.

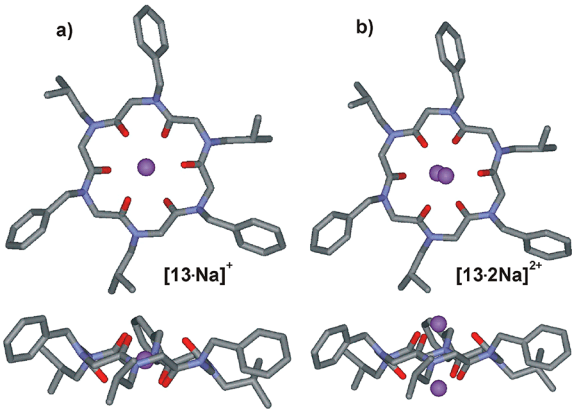

Figure 12. Minimum energy structures (top and side view) of $[\mathbf{13}\cdot Na]^+$ (a) and $[\mathbf{13}\cdot 2Na]^{2+}$ (b). Hydrogen atoms have been omitted for clarity. Atom type: C, gray; N, light blue; O, red; Na^+, magenta.

The remarkable chelating properties of the investigated cyclic peptoids prompted us to attempt crystallization of the NaTFPB complexes in various stoichiometric ratios (1:1 and 1:2 macrocycle/cation) and in different polar and nonpolar solvents ($CHCl_3$, toluene, and acetonitrile). Despite the efforts, we did not succeed in obtaining single crystals suitable for X-ray diffraction. Things changed dramatically by using sodium picrate as the guest.

The addition of two equivalents of this organic salt to a 2:1 chloroform/toluene solution of **13** allowed us to obtain (by slow evaporation) a crystalline yellow solid of **13** as sodium salt complex.

The X-ray analysis showed that the crystals belong to a rather unusual cubic system (a = 27.360(0) Å). The molecular complex is formed in the solid state by six sodium cations, six picrate anions, three cyclopeptoid molecules, and six water molecules. They are aligned along the crystallographic three-fold rotoinversion axis.[44]

As shown in Figure 13, the central cyclopeptoid molecule binds two sodium ions. Each of them is connected by six bridging

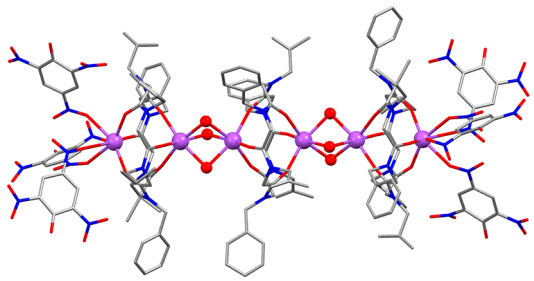

Figure 13. X-ray molecular structure of **13** as sodium complex. Hydrogen atoms and disordered sites have been omitted for clarity. Water oxygen atoms and sodium ions are depicted as ball-and-stick. Atom type: C, gray; N, blue; O, red; Na^+, magenta.

water molecules, to two sodium ions, which bind two cyclopeptoid molecules. Those cyclopeptoid molecules bind two further sodium ions, which complete their coordination sphere by binding three picrate anions each. Interestingly, the picrate anions are linked by means of the oxygen atoms of the nitro group, differently from the analogous strontium picrate cyclopeptoid zwitterion complex, where the phenate oxygen atoms were involved.[4e]

The X-ray molecular structure of the cyclopeptoid molecules features an all-*trans* peptoid bond conformation with the carbonyl groups alternately pointing toward the sodium cations and forcing the N-linked side chains to assume an alternate pseudoequatorial arrangement. Notably, in the case of the beauvericin picrate barium complex a molecular cation is formed with three picrate anions sandwiched between two barium ions.[45] It is worth noting that also for **13** as sodium complex a solvate form is obtained. The chloroform molecules occupy the void space among the molecular complexes, lying on 3-fold rotation axis. Once the complexing abilities of cyclic peptoids **9**–**14** were clarified, we were ready to test their ionophoric properties in liposomes and, eventually, their cytotoxic potentials.

Ion Transport Studies. Enniatins and, in general, cyclic depsipeptides are known ionophores able to transport selectively cations across biological membranes.[6] The best known example is probably valinomycin which transport K^+ with a carrier mechanism and with an impressive selectivity over Na^+ (10^4-fold).[46] However, the activity spectrum is broad, and in the case of enniatins, a passive channel mechanism with a low preference (1.4-fold) for K^+ over Na^+ has been proposed.[12b]

To verify if cyclic peptoids were able to transport cations across a phospholipid membrane, we took advantage of the HPTS assay.[47] In this test, the pH-sensitive fluorescent dye HPTS (8-hydroxypyrene-1,3,6-trisulfonic acid) is trapped in the internal water pool of liposomes (95:5 phosphatidylcholine (PC) and phosphatidylglycerol (PG) lipid composition), and a pH gradient is established across the membrane by external addition of NaOH. The collapse of the transmembrane pH gradient, as a consequence of OH^- influx or H^+ efflux, implies basification of the liposome inner water pool which is signaled by an increase of the HPTS fluorescence emission. To maintain transmembrane electroneutrality, this H^+/OH^- movement has to be balanced by a flux of counterions, which may occur with four possible transport mechanisms: H^+/M^+ or OH^-/X^- antiport and H^+/X^- or OH^-/Na^+ symport. Therefore, the rate of the pH gradient collapse gives direct information on the transportation of H^+/OH^- and indirect information on the correlated symport/antiport of counterions as well as gives information on the efficiency of the ionophore to promote one of the possible transport mechanisms.

A preliminary screening of the compounds panel was made by testing the cation selectivity in ion transport with the HPTS assay, in the presence of the cation under investigation added as the MCl salt. The selectivity test was made for the first group alkali metals, and the kinetic profiles obtained with Na^+ are reported in Figure 14a (see Supporting Information for the results with the other cations). Compound **13** showed the highest activity, whereas all other compounds were almost inactive. In the case of **13**, the selectivity test was extended to anions added as NaX salt (X = Cl^-, Br^-, I^-) and to $CaCl_2$. The overall results of the selectivity experiments are reported in Figure 14b, which compares the normalized fluorescence intensity measured after 300 s of kinetic in the presence of peptoid **13** corrected for the normalized fluorescence intensity measured in the absence of the peptoid (control trace). Analysis of Figure 14b shows similar transport rates in the presence of the different halide anions. In contrast, for cations, there is a strong selectivity for Na^+ and Li^+, whereas for the other cations, values of fluorescence emission close to zero or negative are observed, suggesting that these cations are not transported. This is further confirmed by the slightly negative values of fluorescence emission registered with Rb^+ and Cs^+. This decrease in

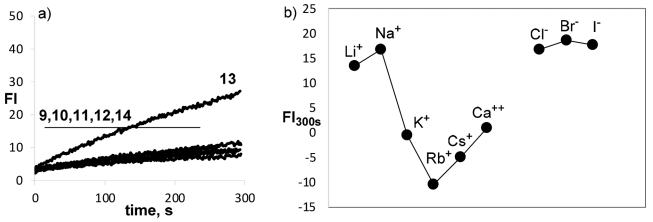

Figure 14. (a) Normalized fluorescence change in HPTS emission (FI) as a function of time after addition of the base (50 μL of 0.5 M NaOH) to 95:5 EYPC/EYPG LUVs (100 nm diameter) loaded with HPTS (0.1 mM HPTS, 0.17 mM total lipid concentration, 25 mM HEPES, 100 mM NaCl, pH 7.0, total volume 3 mL), in the presence of cyclic peptoids **9**–**14**. The concentration of the ionophore is 3 mol % with respect to the total concentration of lipids. (b) Cations and anions selectivity determined for the cyclic peptoid **13** at 5 mol %, using the HPTS assay (100 mM MCl or NaX, pH 7.0, base pulse by addition of 50 μL of 0.5 M MOH). The figure reports the FI measured at 300 s corrected for the FI measured in the absence of the peptoid. The original kinetic profiles and the selectivity tests for compounds **9**–**12** and **14** are reported in the Supporting Information.

fluorescence emission implies an acidification of the inner water pool of the liposomes which is due to an high Na^+/M^+ selectivity in the transport. Indeed, in this experiment, the liposomes are prepared in a buffer containing 100 mM NaCl and then diluted in the buffer containing 100 mM MCl. Therefore, at the beginning of the experiment, when the base pulse is applied, the liposomes contain in the inner water pool Na^+ while outside the concentration of Na^+ is much lower and the concentration of MCl is high. If the ionophore is able to transport both cations, this chemical gradient is easily removed by an antiport of the two cations. This process does not affect the pH of the inner water pool of the liposomes, and therefore, it is not signaled by the HPTS. However, if the ionophore is able to transport only Na^+ (high Na^+/M^+ selectivity), the chemical gradient starts a transport of Na^+ from inside to outside counterbalanced by an antiport of H^+ which results in the acidification of the inner water pool and a lower emission intensity of HPTS (see Figure S29 for a graphical representation or this process).

The observation that the transport rate is independent of the nature of the anion and dependent on the nature of the cation suggests that the inner vesicular pH change signaled by HPTS involves cation transport through an H^+/M^+ antiport or the kinetically equivalent M^+/OH^- symport. To discriminate between this two mechanisms, experiments in the presence of the selective protonophore CCCP (carbonyl cyanide 3-chlorophenylhydrazone) were performed.[48] CCCP is able to transport H^+ in an electrogenic transport process in which $CCCPH^+$ crosses the membrane and, after delivering the proton, it returns back as neutral compounds, thus establishing a unidirectional charge flux. The kinetic profiles of Figure 15b show an impressive acceleration of the transport process induced by the protonophore. This is a strong indication of a H^+/Na^+ antiport mechanism in which the slow step is the antiport of the proton by the ionophore due to a high Na^+/H^+ selectivity. Addition of the protonophore decouples the two processes, thus allowing to fully appreciate the efficacy of the cyclopeptoid in the Na^+ transport (cartoon in Figure 15).

The same acceleration effect is also observed in the case of the other transported cation (Li^+), but the overall cation selectivity profile of **13** remains unchanged (see Supporting Information). Also, in this case, it is evident the acidification effect observed with the nontransported cations, which confirms the high Na^+/M^+ selectivity (see Figures S28e and S29 in the Supporting Information). On the contrary, CCCP has little effect on the transport rate of the other cyclopeptoids with the exception of **14** for which a sizable acceleration and the same cation selectivity is observed (see Supporting Information). The fact that transport activity is observed only for compounds **13** and, although with a much lower efficiency, for **14** is likely related to their high lipophilicity. As a matter of fact, among the compounds investigated only these two have a calculated octanol/water partition coefficient (log*P*) higher than 4 (see Supporting Information). On the other hand, the affinity for the Na^+ ion seems to be less important in influencing the ionophoric activities as demonstrated by the comparison of compounds **12**–**14**, which have very similar logK_a (see Table 2) but log*P* values of 2.9, 4.0, and 4.9, respectively. Although limited to only three compounds, this bell-shaped correlation between transport activity and carrier lipophilicity, with an optimal value in our case corresponding to that of compound **13**, is frequently observed in carrier type ion transporters. This behavior is interpreted as a balance between the need to form a lipophilic complex able to cross the membrane and the need for the ionophore to approach the membrane/water interphase where the ion exchange process occurs.[49]

To further investigate the mechanism of transport of cyclopeptoid **13**, a series of kinetic experiments at different concentration of ionophore in the absence and in the presence of CCCP were performed. Figure 16a reports the first-order rate constants (k_t, s^{-1}) for the transport process, obtained by the fitting of the kinetic profiles reported in the Supporting Information, plotted against the concentration of ionophore. In both cases, a linear dependence is observed, and this suggests that

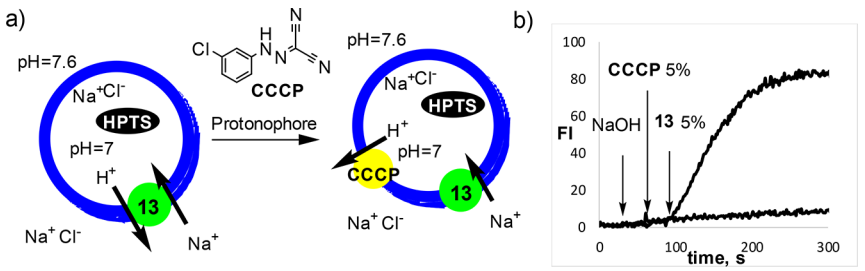

Figure 15. (a) Schematic representation of the HPTS assay in the presence of the CCCP protonophore. (b) Normalized fluorescence change in HPTS emission as a function of time after addition of the base at 25 s (50 μL of 0.5 M NaOH), the CCCP protonophore at 50 s (5 μL 5.2 mM in DMSO), and the cyclic peptoid **13** at 90 s to 95:5 EYPC/EYPG LUVs (100 nm diameter) loaded with HPTS (0.1 mM HPTS, 0.17 mM total lipid concentration, 25 mM HEPES, 100 mM NaCl, pH 7.0, total volume 3 mL). The concentration of the ionophore is 5 mol % with respect to the total concentration of lipids. The slower kinetic is made in the same conditions but without the addition of **13**.

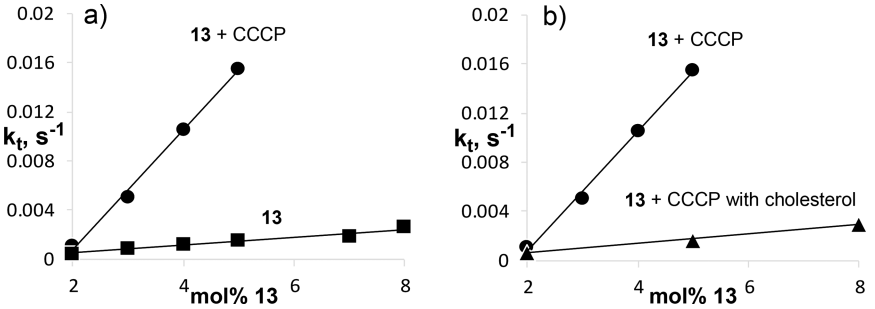

Figure 16. (a) Dependence of k_t on the concentration of cyclopeptoid **13** in the absence (■) and in the presence of the CCCP protonophore (5%, ●) and (b) dependence of k_t on the concentration of cyclopeptoid **13** in the presence of 5 mol % of CCCP with cholesterol (EYPC/PG/CHOL 66.5:3.5:30,▲) and without cholesterol (PC/PG 95:5, ●).

the transport active species is monomeric, in our case a 1:1 [**13**·Na]$^+$ complex. Hill analysis of the kinetic profiles was performed to obtain the EC_{50}, which represent the "effective" peptoid concentration needed to reach 50% activity (see Supporting Information).[50] EC_{50} values for compounds **13** of 3.91 ± 0.26 and 1.69 ± 0.08% were obtained in the absence and presence of CCCP, respectively. Transforming the concentration from % to lipid to molarity, these values correspond to a 6.65 and 2.88 μM ionophore concentration. Interestingly, the Hill coefficient (n) increases from 1.04 ± 0.15 to 1.65 ± 0.12 on addition of CCCP, confirming that **13** alone acts as a monomeric species but suggesting some participation of complexes with a 2:1 ligand/metal ion stoichiometry to the transport process in the presence of the protonophore.

Finally, the activity of **13** using liposomes containing cholesterol (66.5:3.5:30 PC/PG/cholesterol lipid composition) was investigated. Cholesterol is known to rigidify the phospholipidic membrane and it is used to discriminate transport mechanisms because, in a more rigid membrane environment, the activity of a mobile carrier should decrease while that of a channel system, which does not move in the membrane, should be unaffected.[51] In Figure 16b are reported the first-order rate constants (k_t, s^{-1}) for the transport process with or without cholesterol, and a significant decrease of activity is associated with the presence of cholesterol. This result is a clear indication that cyclopeptoid **13** transports Na^+ with a mobile carrier mechanism, which is further reinforced by the observation that the active species is essentially monomeric and by the dependence of the transport activity from the lipophilicity of the carrier.

The indication of a carrier H^+/Na^+ antiport mechanism demonstrated for **13** is particularly interesting considering that the acute toxicity of enniatins is related to the mitochondrial collapse of the cellular energy metabolism.[10b,52] The perturbation of the cation gradient across the inner mitochondrial membrane is, in fact, vital for the ATP production. These results were considered propitious for the scheduled cytotoxic assays.

Cytotoxic Activities. On the basis of the ability of beauvericin to induce cytotoxicity in different cancer cell lines, such as MIA Pa Ca-2 (pancreatic carcinoma), MCF-7 (breast), SF-268 (CNS glioma), PC-3 (prostate cancer),[53,54] and driven by the promising results of the ion transport studies, we decided to evaluate the potential anti-proliferative or cytotoxic activity of cyclic peptoids **9**−**14** in PC-3 human metastatic prostate cancer and in A375 human melanoma cell lines. We also tested the linear zwitterionic peptoids **15**−**19** in order to unambiguously establish the importance of the cyclization for the biological activities. The cell lines were incubated for 72 h with increasing concentration of the compounds (2−50 μM), and cell viability was determined by MTT proliferation assay.

Under the same experimental conditions, while none of the linear peptoids show any cytotoxic activity, four cyclic congeners (**11**−**14**) affected the cancer cell vitality with activities (IC_{50}) in the μM range with potencies 5−19 times lower than that of the natural beauvericin, used as control in both cancer cell lines (see Table 3).

Table 3. IC_{50} Values of Cyclic Peptoids 9−14 and Beauvericin in Human Cancer Cell Lines after 72 h Treatment

cyclic peptoid	PC-3 prostate cell line	A375 melanoma cell line
9	NA[a]	NA[a]
10	NA[a]	NA[a]
11	25.4 ± 1.5	22.7 ± 1.2
12	28.4. ± 2.1	30.1 ± 2.3
13	9.5 ± 0.8	8.3 ± 1.1
14	21.0 ± 1.2	19.1 ± 1.6
beauvericin (**8**)	1.5 ± 0.2	1.6 ± 0.1

[a]NA: not active.

Among the tested compounds, **13**, showing alternated benzyl/isobutyl side chains, exhibited the strongest antiproliferative effect on both A375 and PC-3 cell lines, with IC_{50} values of 8.3 ± 1.1 and 9.5 ± 0.8 μM, respectively. We, thus, selected **13** to perform further investigations in order to shed light on its possible mechanism of action. For this purpose, A375 and PC-3 cells were incubated for 72 h with compound **13** used at a concentration close to its IC_{50} value and at higher doses (5, 10, and 20 μM) and analyzed by flow cytometry. Beauvericin (**8**) was used in the same conditions with a concentration close to its IC_{50} value. For cyclic peptoid **13**, in both cancer cell lines, we observed that the phase S significantly increased (between 7 and 18% in a dose-dependent manner), while the G_0/G_1 phase decreased, without any significant increase of hypodiploid SubG1 cells, compared to the control cells (Figure 17a,b). Beauvericin (**8**), tested in the same conditions showed a similar behavior, in fact after exposure to beauvericin for 72 h, we detected a substantial increase of the S and G_2/M phase cell fraction, with a reduction of cells in G_0/G_1 phase with respect to the control, in accordance with the data reported for the same compound on other cancer cell lines.[55,56]

Furthermore, in contrast with compound **13**, the treatment with beauvericin caused an increase of sub-G_1 population indicative of apoptotic/necrotic cell death, in accordance with published results.[55,56]

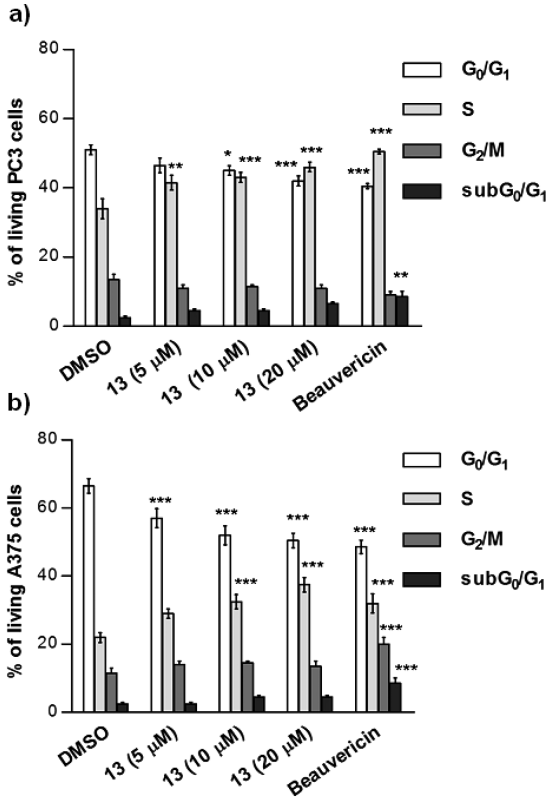

Figure 17. Effects of compound **13** and beauvericin (**8**) on cell cycle progression. Cell distribution in the different phases of the cell cycle was analyzed by flow cytometry (A, PC-3 cells; B, 375 cells). PI stained viable PC-3 or A375 cells treated with DMSO; compound **13** (5, 10, 20 μM) or beauvericin (**8**) (2 μM) for 72 h. Results are expressed as means ± SD of three experiment performed in triplicate (***$P < 0.001$, **$P < 0.005$, *$P < 0.05$).

CONCLUSIONS

The design of molecules capable of mimicking bioactive natural products represents a promising strategy for the modulation and exploration of fundamental biological processes. For their malleable structure, the ease of synthesis, and the high diversity attainable, cyclic peptoids have proven to be an excellent scaffold for the mimicry of Nature's designed oligomers. In this contribution, we demonstrate that variants of cyclic hexameric peptoids (decorated with N-linked isopropyl, isobutyl, and benzyl groups) structurally resemble, as sodium ion complexes, the natural mycotoxins, enniatins and beauvericin. By mixing different side chains, in order to better understand the morphology/lipophilicity impact, we showed that there is a delicate balance between structure and activity. To the best of our knowledge, **13** (devoid of formal natural counterpart) represents the first example of highly cytotoxic cyclic peptoid. It exhibits a clear correlation between sodium transport ability and cytotoxic activities on human cancer cell lines. The indication of a carrier H^+/Na^+ antiport mechanism suggests the mitochondrial metabolism as possible target (as demonstrated in the case of enniatins).

Furthermore, the structural studies performed on the side-chain-alternated cyclic oligomers shed light on the neglected conformational chirality associated with their shape.

The proper use of this information and the intrinsic properties of the intriguing peptoid scaffold represent a starting point for further investigations in the vast field of biomimetics and for progress in structural/biomedical research.

EXPERIMENTAL SECTION

Synthesis. *General Methods.* Starting materials and reagents purchased from commercial suppliers were generally used without purification unless otherwise mentioned. HPLC analyses were performed on a JASCO LC-NET II/ADC equipped with a JASCO model PU-2089 Plus Pump and a JASCO MD-2010 Plus UV−vis multiple wavelength detector set at 220 nm. The column used was a C_{18} reversed-phase analytical column (Waters, Bondapak, 10 μm, 125 Å, 3.9 mm × 300 mm) run with linear gradients of ACN (0.1% TFA) into H_2O (0.1% TFA) over 30 min, at a flow rate of 1.0 mL/min for the analytical runs. ESI-MS analysis in positive ion mode was performed using a Finnigan LCQ Deca ion trap mass spectrometer (ThermoFinnigan, San Jose, CA, USA), and the mass spectra were acquired and processed using the Xcalibur software provided by Thermo Finnigan. Samples were dissolved in 1:1 CH_3OH/H_2O, 0.1% formic acid, and infused in the ESI source by using a syringe pump; the flow rate was 5 μL/min. The capillary voltage was set at 4.0 V, the spray voltage at 5 kV, and the tube lens offset at −40 V. The capillary temperature was 220 °C. The samples of the bis-sodiated adducts were dissolved in acetonitrile and infused in the ESI source by using a syringe pump. Data were acquired in MS^1 and MS^n scanning modes. Zoom scan was used in these experiments. High-resolution mass spectra (HRMS) were recorded on a Bruker Solarix XR Fourier transform ion cyclotron resonance mass spectrometer (FTICR-MS) equipped with a 7 T magnet, using electrospray ionization (Supporting Information). Yields refer to chromatographically and spectroscopically (^{1}H and ^{13}C NMR) pure materials. NMR spectra were recorded on a Bruker DRX 600 (^{1}H at 600.13 MHz, ^{13}C at 150.90 MHz) and a Bruker DRX 400 (^{1}H at 400.13 MHz, ^{13}C at 100.03 MHz). Chemical shifts (δ) are reported in parts per million relative to the residual solvent peak ($CHCl_3$, $\delta = 7.26$; $^{13}CDCl_3$, $\delta = 77.00$; C_2DHCl_4, TCDE, $\delta = 6.00$), and the multiplicity of each signal is designated by the following abbreviations: s, singlet; d, doublet; dd, double doublet; t, triplet; sept, septet; m, multiplet; br, broad. 2D NMR experiments such as COSY, ROESY, HSQC, and HMBC were performed for the full assignment of each signal. Coupling constants (J) are quoted in hertz. See list of abbreviations in the Supporting Information.

*General Procedure for the "Submonomer" Solid-Phase Synthesis of Linear Peptoids **15**−**19**.* The 2-chlorotrityl chloride resin (α-dichlorobenzhydryl-polystyrene cross-linked with 1% DVB; 100−200 mesh; 1.63 mmol g^{-1}, 0.400 g, 0.652 mmol) was swelled in dry CH_2Cl_2 (4 mL) for 45 min and washed twice with dry CH_2Cl_2 (4 mL). The first submonomer was attached onto the resin by adding bromoacetic acid (0.136 g, 0.978 mmol) in dry CH_2Cl_2 (4 mL) and DIPEA (567 μL, 3.26 mmol) on a shaker platform for 60 min at room temperature, followed by washing with CH_2Cl_2 (3 × 1 min) and then again with DMF (3 × 1 min). A solution of the chosen amine (1.6 M in dry DMF, 4 mL) was added to the bromoacetylated resin. The mixture was left on a shaker platform for 30 min at room temperature, then the resin was washed with DMF (3 × 1 min), CH_2Cl_2 (3 × 1 min), and then again with DMF (3 × 1 min). Subsequent bromoacetylation reactions were accomplished by reacting the aminated oligomer with a solution of bromoacetic acid (0.910 g, 6.52 mmol) and DIC (1.11 mL), 7.17 mmol) in dry DMF (4 mL) for 40 min at room temperature. The filtrated resin was washed with DMF (4 × 1 min), CH_2Cl_2 (4 × 1 min), DMF (4 × 1 min), and treated again with the proper amine under the same conditions reported above. This cycle of reactions was iterated until the target hexamer was obtained. The cleavage was performed treating the resin, previously washed with CH_2Cl_2 (3 × 1 min), twice with a solution of HFIP in CH_2Cl_2 (20% v/v, 5.0 mL each time) on a shaker platform at room temperature for 30 and 5 min, respectively. The resin was then filtered away, and the combined filtrates were concentrated in vacuo. Two milligrams of the final products was dissolved in 200 μL of acetonitrile (0.1% TFA) and 200 μL of HPLC grade water (0.1% TFA) and analyzed by RP-HPLC; purity >95%; conditions: 5 → 100% A in 30 min for the all oligomers (A, 0.1% TFA in acetonitrile, B, 0.1% TFA in water); flow: 1.0 mL min^{-1}, 220 nm]. The linear oligomers (isolated as amorphous

solids) were subjected to ESI mass spectrometry and, subsequently, to the cyclization reactions without further purification.

H-[*N*Val]$_6$-OH (**15**): white amorphous solid, 0.495 g, 100%; t_R = 9.6 min; ES-MS *m/z* 613.0 [M + H]$^+$; HRMS (ESI/FTICR) *m/z* [M + H]$^+$ calcd for $C_{30}H_{57}N_6O_7^+$ 613.4283; found 613.4289.

H-[*N*Leu-*N*Val]$_3$-OH (**16**): white amorphous solid, 0.392 g, 92%; t_R = 9.9 min; ES-MS *m/z* 655.1 [M + H]$^+$; HRMS (ESI/FTICR) *m/z* [M + H]$^+$ calcd for $C_{33}H_{63}N_6O_7^+$ 655.4753; found 655.4741.

H-[*N*Phe-*N*Val]$_3$-OH (**17**): white amorphous solid, 0.430 g, 87%; t_R = 10.0 min; ES-MS *m/z* 757.2 [M + H]$^+$; HRMS (ESI/FTICR) *m/z* [M + H]$^+$ calcd for $C_{42}H_{57}N_6O_7^+$ 757.4283; found 757.4278.

H-[*N*Leu]$_6$-OH (**18**): white amorphous solid, 0.343 g, 76%; t_R = 10.1 min; ES-MS *m/z* 697.0 [M + H]$^+$; HRMS (ESI/FTICR) *m/z* [M + H]$^+$ calcd for $C_{36}H_{69}N_6O_7^+$ 697.5222; found 697.5211.

H-[*N*Phe-*N*Leu]$_3$-OH (**19**): white amorphous solid, 0.406 g, 78%; t_R = 10.8 min; ES-MS *m/z* 799.0 [M + H]$^+$; HRMS (ESI/FTICR) *m/z* [M + H]$^+$ calcd for $C_{45}H_{63}N_6O_7^+$ 799.4753; found 799.4749.

General Procedure for the High Dilution Cyclization. Synthesis of Cyclic Peptoids ***9*****–*****13***. The solutions of the linear peptoids (0.150 mmol), previously coevaporated three times with toluene, were prepared under nitrogen in dry CH_2Cl_2 (5.0 mL). The mixture was added dropwise to a stirred solution of HATU (0.171 g, 0.450 mmol) and DIPEA (105 μL, 0.600 mmol) in dry DMF (45.0 mL) by a syringe pump in 6 h, at room temperature in anhydrous atmosphere. After 18 h, the resulting mixture was concentrated in vacuo, diluted with CH_2Cl_2 (30 mL), and washed with a solution of HCl (1.0 M, 15 mL). The mixture was extracted with CH_2Cl_2 (2 × 30.0 mL), and the combined organic phases were washed with water (30.0 mL), dried over anhydrous $MgSO_4$, filtered, and concentrated in vacuo. The cyclic peptoids were dissolved in 50% acetonitrile in HPLC grade water and analyzed by RP-HPLC; purity >95% conditions: 5−100% A in 30 min (A, 0.1% TFA in acetonitrile, B, 0.1% TFA in water); flow: 1 mL min^{-1}, 220 nm. The crude cyclic peptoids **9** and **10**−**13** were dissolved in hot acetonitrile and precipitated by slowly cooling the acetonitrile solutions. The crude **10** was purified on reverse silica gel (C_{18}); conditions: 10−100% A (A: acetonitrile; B: water).

cyclo-[*N*Val]$_6$ (**9**): white amorphous solid, 0.032 g, 36%; t_R = 10.7 min; ^{1}H NMR (600 MHz, $CDCl_3$, mixture of rotamers) δ 4.91−3.18 (18H, overlapping, O=C−C*H*$_2$-N, −C*H*(CH$_3$)$_2$), 1.47−0.93 (36H, overlapping, −CH(C*H*$_3$)$_2$); ^{13}C NMR (150 MHz, $CDCl_3$, mixture of rotamers) δ 171.0, 170.6, 170.1, 169.4, 169.0, 168.3, 167.4, 167.3, 48.5, 48.0, 47.8, 46.1, 45.9, 45.5, 45.4, 44.8, 44.0, 43.5, 43.4, 43.3, 43.2, 43.1, 42.5, 21.8, 21.6, 21.5, 21.2, 20.9, 20.6, 20.4, 20.3, 19.9, 19.5, 19.4, 19.1; ESI-MS *m/z* 595.1 (100, [M + H]$^+$); 617.2 (95, [M + Na]$^+$); HRMS (ESI/FTICR) *m/z* [M + H]$^+$ calcd for $C_{30}H_{55}N_6O_6^+$ 595.4178; found 595.4178.

cyclo-[*N*Val-*N*Leu]$_3$ (**10**): white amorphous solid, 0.062 g, 65%; t_R = 11.4 min; ^{1}H NMR (600 MHz, $CDCl_3$, mixture of rotamers) δ 4.81−2.85 (21H, overlapping, br signals, O=C−C*H*$_2$-N, N−C*H*(CH$_3$)$_2$, −C*H*$_2$−CH(CH$_3$)$_2$), 2.12−1.82 (3H, overlapping, br signals, −CH$_2$−C*H*(CH$_3$)$_2$), 1.43−0.97 (36H, overlapping, br signals, −CH(C*H*$_3$)$_2$), −CH$_2$−CH(C*H*$_3$)$_2$; ^{13}C NMR (150 MHz, $CDCl_3$, mixture of rotamers) δ 171.8, 171.5, 171.0, 170.2, 169.7, 169.4, 169.0, 168.6, 168.0, 167.6, 167.3, 166.9, 57.2, 57.0, 56.8, 56.4, 56.1, 55.8, 52.1, 49.8, 49.5, 49.3, 48.5, 48.2, 48.0, 47.8, 47.6, 45.9, 45.7, 45.1, 44.4, 43.1, 42.8, 28.0, 27.3, 27.1, 21.2, 20.1, 19.5, 19.3; ESI-MS *m/z* 637.4 (45 [M + H]$^+$); 659.3 (100 [M + Na]$^+$); HRMS (ESI/FTICR) *m/z* [M + H]$^+$ calcd for $C_{33}H_{61}N_6O_6^+$ 637.4647; found 637.4661.

cyclo-[*cis*-*N*Val^1-*cis*-*N*Phe^1-*trans*-*N*Val^2-*cis*-*N*Phe^2-*cis*-*N*Val^3-*trans*-*N*Phe^3] (**11**): white amorphous solid, 0.050 g, 45%; t_R = 11.5 min; NMR data are reported in Table 1; ESI-MS *m/z* 761.4 (100 [M + H + Na]$^+$); 739.2 (10 [M + H]$^+$); HRMS (ESI/FTICR) *m/z* [M + H]$^+$ calcd for $C_{42}H_{55}N_6O_6^+$ 739.4178; found 739.4178.

cyclo-[*N*Leu]$_6$ (**12**): white amorphous solid, 0.061 g, 60%; t_R = 10.9 min; ^{1}H NMR (600 MHz, $CDCl_3$, mixture of rotamers) δ 4.68−3.08 (24H, overlapping, br signals, O=C−C*H*$_2$-N, −C*H*$_2$−CH(CH$_3$)$_2$), 2.15−1.79 (6H, overlapping, br signals, −CH$_2$−C*H*(CH$_3$)$_2$), 0.99−0.86 (36H, overlapping, br signals, −CH(C*H*$_3$)$_2$); ^{13}C NMR (150 MHz, $CDCl_3$, mixture of rotamers) δ 171.4, 170.9, 170.5, 169.9, 169.7, 169.5, 168.9, 168.8, 168.6, 168.5, 168.0, 167.5, 57.1, 57.0, 56.7, 56.6, 56.3, 56.0, 55.9, 55.5, 55.2, 53.5, 51.7, 49.9, 49.6, 49.5, 49.2, 49.1, 49.0, 48.6, 48.1, 46.4, 28.2, 28.1, 28.0, 27.7, 27.5, 27.3, 27.2, 27.1, 27.0, 26.5, 20.2, 20.0; ESI-MS *m/z* 679.3 (90 [M + H]$^+$); 701.2 (100 [M + Na]$^+$); HRMS (ESI/FTICR) *m/z* [M + H]$^+$ calcd for $C_{36}H_{67}N_6O_6^+$ 679.5117; found 679.5102.

cyclo-[*N*Phe-*N*Leu]$_3$ (**13**): white amorphous solid, 0.056 g, 48%; t_R = 12.8 min; ^{1}H NMR (600 MHz, $CDCl_3$, mixture of rotamers) δ 7.57−7.03 (15H, overlapping, br signals, Ar-*H*), 5.51−2.84 (24H, overlapping, br signals, O=C−C*H*$_2$−N, C*H*$_2$−Ph, −C*H*$_2$−CH(CH$_3$)$_2$), 2.16−1.71 (3H, overlapping, br signals, −CH$_2$−C*H*(CH$_3$)$_2$), 0.95−0.92 (18H, overlapping, br signals, −CH(C*H*$_3$)$_2$); ^{13}C NMR (150 MHz, $CDCl_3$, mixture of rotamers) δ 171.8, 171.5, 170.3, 169.6, 169.5, 168.5, 167.5, 137.0, 136.6, 135.3, 129.1, 128.8, 128.7, 128.4, 128.0, 127.8, 127.7, 127.4, 127.2, 126.9, 125.5, 56.7, 56.5, 56.1, 52.8, 51.7, 51.6, 51.5, 50.8, 50.3, 49.8, 49.5, 49.2, 48.7, 47.6, 27.6, 27.3, 20.1, 20.0; ESI-MS *m/z* 781.1 (10 [M + H]$^+$); 803.1 (100 [M + Na]$^+$); HRMS (ESI/FTICR) *m/z* [M + H]$^+$ calcd for $C_{45}H_{61}N_6O_6^+$ 781.4647; found 781.4653.

*General Procedure for the Monometallic Complex Formation [****9*****–*****14****·Na]$^+$[TFPB]$^-$*. To 1.0−10.0 mM (depending on the solubility) solutions of **9**−**14** in $CDCl_3$ (0.5 mL) were added increasing amounts of NaTFPB until 1.0 equiv (depending on the titration, see Supporting Information). After any addition, the mixtures were sonicated for 5 min and the NMR spectra were recorded.

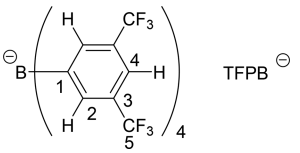

[**9**·Na]$^+$TFPB$^-$: ^{1}H NMR (600 MHz, $CDCl_3$) δ 7.70 (8H, s, TFPB-*o*-*H*), 7.53 (4H, s, TFPB-*p*-*H*), 4.51 (6H, d, *J* 17.2 Hz, O=C−C*H*H−N), 4.06 (6H, ept, *J* 6.4 Hz, −C*H*(CH$_3$)$_2$), 3.66 (6H, d, *J* 17.2 Hz, O=C−CH*H*-N), 1.20 (18 H, d, *J* 6.4 Hz, −CH(C*H*$_3$)(CH$_3$)), 1.18 (18 H, d, *J* 6.4 Hz, −CH(CH$_3$)(C*H*$_3$)); ^{13}C NMR (150 MHz, $CDCl_3$:CD_3CN 4:1, the CD_3CN was added to avoid precipitation of the salt) δ 169.1 (*C*=O), 161.6 (q, *J* 50 Hz, C-1), 134.8 (C-2), 128.8 (q, *J* 30 Hz C-3), 124.6 (q, *J* 270 Hz, C-5), 117.4 (C-4), 48.0 (O=C-CH$_2$−N), 42.9 (−CH(CH$_3$)$_2$), 21.6 (−CH$_3$), 20.0 (−CH$_3$); ESI-MS *m/z* 617.3 [M + Na]$^+$.

[**10**·Na]$^+$TFPB$^-$: ^{1}H NMR (600 MHz, $CDCl_3$) δ 7.70 (8H, s, TFPB-*o*-*H*), 7.52 (4H, s, TFPB-*p*-*H*), 4.74 (3H, d, *J* 16.2 Hz, O=C−C*H*H−N-*i*Bu), 4.51 (3H, d, *J* 16.1 Hz, O=C−C*H*H−N-*i*Pr), 3.98 (3H, ept, *J* 6.3 Hz, −C*H*(CH$_3$)$_2$), 3.61 (3H, d, *J* 16.1 Hz, O=C−CH*H*-N-*i*Pr), 3.54 (3H, d, *J* 16.2 Hz, O=C−CH*H*-N-*i*Bu), 3.26 (3H, dd, *J* 14.0 and 7.0 Hz, −C*H*H−CH(CH$_3$)$_2$), 3.01 (3H, dd, *J* 14.0 and 7.0 Hz, −CH*H*−CH(CH$_3$)$_2$), 1.84 (3H, m, −CH$_2$−C*H*(CH$_3$)$_2$), 1.19 (9H, d, *J* 6.3 Hz, −CH(C*H*$_3$)(CH$_3$)), 1.16 (9H, d, *J* 6.3 Hz, −CH(CH$_3$)(C*H*$_3$)), 1.01 (9H, d, *J* 6.7 Hz, −CH$_2$−CH(C*H*$_3$)(CH$_3$)), 0.90 (9H, d, *J* 6.7 Hz, −CH$_2$−CH(CH$_3$)(C*H*$_3$)); ^{13}C NMR (150 MHz, $CDCl_3$) δ 168.9 (*C*=O), 167.0 (*C*=O), 161.1 (q, *J* 50 Hz, C-1), 134.2 (C-2), 128.3 (q, *J* 30 Hz C-3), 124.0 (q, *J* 270 Hz, C-5), 117.0 (C-4), 56.2 (−CH$_2$−CH(CH$_3$)$_2$), 48.9 (O=C-CH$_2$−N), 47.6 (O=C-CH$_2$−N), 42.1 (N-CH(CH$_3$)$_2$), 27.2 (−CH$_2$−CH(CH$_3$)$_2$), 20.6 (−CH$_3$), 19.4 (−CH$_3$), 19.3 (−CH$_3$), 19.2 (−CH$_3$); ESI-MS *m/z* 659.4 [M + Na]$^+$.

[**11**·Na]$^+$TFPB$^-$: ^{1}H NMR (600 MHz, $CDCl_3$) δ 7.70 (8H, s, TFPB-*o*-*H*), 7.50 (4H, s, TFPB-*p*-*H*), 7.40 (6H, t, *J* 7.0 Hz, Ar-*m*-*H*), 7.36 (3H, t, *J* 7.0 Hz, Ar-*p*-*H*), 7.22 (6H, d, *J* 7.0 Hz, Ar-*o*-*H*), 4.88 (3H, d, *J* 16.0 Hz, N−C*H*H-Ph), 4.77 (3H, d, *J* 17.0 Hz, O=C−C*H*H−N−Bn), 4.65 (3H, d, *J* 17.0 Hz, O=C−C*H*H−N-*i*Pr), 4.39 (3H, d, *J* 16.0 Hz, N−CH*H*-Ph), 3.89 (3H, ept, *J* 6.3 Hz, −C*H*(CH$_3$)$_2$), 3.60 (3H, d, *J* 17.0 Hz, O=C−CH*H*-N-*i*Pr), 3.57 (3H, d, *J* 17.0 Hz, O=C−CH*H*-N-Bn), 1.15 (9H, d, *J* 6.3 Hz, −CH(C*H*$_3$)(CH$_3$)), 1.05 (9H, d, *J* 6.3 Hz, −CH(CH$_3$)(C*H*$_3$)); ^{13}C NMR (150 MHz, $CDCl_3$) δ 171.5 (C=O), 168.4 (C=O), 161.7 (q, *J* 50 Hz, C-1), 134.8 (CH-Ph), 134.6 (C-2), 129.4 (CH-Ph), 128.9 (q, *J* 30 Hz C-3), 128.7 (CH-Ph), 126.9 (CH-Ph), 124.6 (q, *J* 270 Hz, C-5), 117.4 (C-4), 53.1 (CH$_2$-benzyl), 48.9 (O=C-CH$_2$−N), 48.1 (O=C-CH$_2$−N), 43.1 (−CH(CH$_3$)$_2$), 21.3 (−CH$_3$), 20.0 (−CH$_3$); ESI-MS *m/z* 761.3 [M + Na]$^+$.

[**12**·Na]$^+$TFPB$^-$: ^{1}H NMR (600 MHz, $CDCl_3$) δ 7.70 (8H, s, TFPB-*o*-*H*), 7.52 (4H, s, TFPB-*p*-*H*), 4.75 (6H, d, *J* 17.2 Hz, O=C−C*H*H−N-

*i*Bu), 3.50 (6H, d, *J* 17.2 Hz, O=C−CH*H*-N-*i*Bu), 3.18 (6H, dd, *J* 14.0 and 6.0 Hz, −C*H*H−CH(CH_3)$_2$), 3.02 (6H, dd, *J* 14.0 and 6.0 Hz, −CH*H*−CH(CH_3)$_2$), 1.83 (6H, m, −CH_2−C*H*(CH_3)$_2$), 1.00 (18H, d, *J* 6.4 Hz, −CH_2−CH(*C*H_3)(CH_3)), 0.92 (18H, d, *J* 6.4 Hz, −CH_2−CH(CH_3)(*C*H_3)); ^{13}C NMR (150 MHz, $CDCl_3$) *δ* 170.2 (*C*=O), 161.7 (q, *J* 50 Hz, C-1), 134.8 (C-2), 128.8 (q, *J* 30 Hz C-3), 124.6 (q, *J* 270 Hz, C-5), 117.4 (C-4), 57.0 (−*C*H_2−CH(CH_3)$_2$), 49.9 (O=C-*C*H_2−N), 27.9 (−CH_2−*C*H(CH_3)$_2$), 20.2 (−CH_3), 20.0 (−CH_3); ESI-MS *m*/*z* 701.2 [M + Na]$^+$.

[**13**·Na]$^+$TFPB$^-$: ^{1}H NMR (600 MHz, $CDCl_3$) *δ* 7.71 (8H, s, TFPB-*o*-*H*), 7.51 (4H, s, TFPB-*p*-*H*), 7.38 (6H, t, *J* 7.0 Hz, Ar-*m*-*H*), 7.34 (3H, t, *J* 7.0 Hz, Ar-*p*-*H*), 7.22 (6H, d, *J* 7.0 Hz, Ar-*o*-*H*), 4.91 (3H, d, *J* 17.0 Hz, N−C*H*H-Ph), 4.80 (3H, d, *J* 17.4 Hz, O=C−C*H*H−N−Bn), 4.74 (3H, d, *J* 17.4 Hz, O=C−C*H*H−N-*i*Bu), 4.39 (3H, d, *J* 17.0 Hz, N−CH*H*-Ph), 3.53 (3H, d, *J* 17.4 Hz, O=C−CH*H*-N-*i*Bu), 3.50 (3H, d, *J* 17.4 Hz, O=C−N−CH*H*-N-Bn), 3.05 (3H, dd, *J* 14.0 and 6.0 Hz, −C*H*H−CH(CH_3)$_2$), 2.98 (3H, dd, *J* 14.0 and 6.0 Hz, −CH*H*−CH(CH_3)$_2$), 1.72 (3H, m, −CH_2−C*H*(CH_3)$_2$), 0.95 (9H, d, *J* 6.0 Hz, −CH_2−CH(*C*H_3)(CH_3)), 0.77 (9H, d, *J* 6.0 Hz, −CH_2−CH(CH_3)-(*C*H_3)); ^{13}C NMR (150 MHz, $CDCl_3$) *δ* 171.1 (*C*=O), 169.9 (*C*=O), 161.7 (q, *J* 50 Hz, C-1), 134.8 (C-2), 134.1 (*C*-Ph), 129.4 (*C*H-Ph), 128.9 (q, *J* 30 Hz C-3), 128.8 (*C*H-Ph), 127.4 (*C*H-Ph), 124.6 (q, *J* 270 Hz, C-5), 117.4 (C-4), 56.7 (−*C*H_2−CH(CH_3)$_2$), 52.9 (*C*H_2-benzyl), 49.9 (O=C-*C*H_2−N), 49.2 (O=C-*C*H_2−N), 27.8 (−CH_2−*C*H-(CH_3)$_2$), 20.0 (−CH_3), 19.8 (−CH_3); ESI-MS *m*/*z* 803.1 [M + Na]$^+$.

[**14**·Na]$^+$TFPB$^-$: ^{1}H NMR (600 MHz, $CDCl_3$) *δ* 7.71 (8H, s, TFPB-*o*-*H*), 7.50 (4H, s, TFPB-*p*-*H*), 7.40 (18H, m, Ar-*m*-*H* and Ar-*p*-*H*), 7.09 (12H, d, *J* 7.0 Hz, Ar-*o*-*H*), 4.86 (6H, d, *J* 17.3 Hz, O=C−CH*H*-), 4.65 (6H, d, *J* 16.2 Hz, N−C*H*H-Ph), 4.35 (6H, d, *J* 16.2 Hz, N−CH*H*-Ph), 3.53 (6H, d, *J* 17.3 Hz, O=C−C*H*H−); ^{13}C NMR (150 MHz, $CDCl_3$) *δ* 169.4 (*C*=O), 161.7 (q, *J* 50 Hz, C-1), 134.8 (C-2), 132.9 (*C*-Ph), 129.6 (*C*H-Ph), 128.9 (q, *J* 30 Hz C-3), 128.8 (*C*H-Ph), 128.3 (q, *J* 270 Hz, C-5), 125.4 (*C*H-Ph), 117.6 (C-4), 53.0 (*C*H_2-benzyl), 49.0 (O=C-*C*H_2−N); ESI-MS *m*/*z* 906.3 [M + Na]$^+$.

*General Procedure for the Bimetallic Complex Formation [**10**−**14**·2Na]$^{2+}$2[TFPB]$^-$.* To 1.0 mM solutions of **9**−**14** in $CDCl_3$ (0.5 mL), were added 2.0 equiv of NaTFPB. After any addition, the mixtures were sonicated for 10 min and the NMR spectra were recorded (see Supporting Information). Only in the case of the cyclic peptoid **9** we obtained the same spectrum reported for [**9**·Na]$^+$TFPB$^-$ (there was no appreciable formation of the bimetallic complex). The low solubility of [**10**−**12**,**14**·2Na]$^{2+}$2TFPB$^-$ hampered the acquisition of their ^{13}C NMR specra.

[**10**·2Na]$^{2+}$2TFPB$^-$:^{1}H NMR (600 MHz, $CDCl_3$) *δ* 7.55 (16H, s, TFPB-*o*-*H*), 7.43 (8H, s, TFPB-*p*-*H*), 4.49 (3H, d, *J* 16.7 Hz, O=C−C*H*H−N-*i*Bu), 4.28 (3H, d, *J* 16.6 Hz, O=C−C*H*H−N-*i*Pr), 3.93 (3H, ept, *J* 6.3 Hz, −C*H*(CH_3)$_2$), 3.54 (3H, d, *J* 16.6 Hz, O=C−CH*H*-N-*i*Pr), 3.53 (3H, d, *J* 16.7 Hz, O=C−CH*H*-N-*i*Bu), 3.14 (3H, dd, *J* 14.3 and 6.2 Hz, −C*H*H−CH(CH_3)$_2$), 2.93 (3H, dd, *J* 14.3 and 6.0 Hz, −CH*H*−CH(CH_3)$_2$), 1.78 (3H, m, −CH_2−C*H*(CH_3)$_2$), 1.08 (9H, d, *J* 6.3 Hz, −CH(*C*H_3)(CH_3)), 1.02 (9H, d, *J* 6.3 Hz, −CH(CH_3)(*C*H_3)), 0.88 (9H, d, *J* 6.2 Hz, −CH_2−CH(*C*H_3)(CH_3)), 0.82 (9H, d, *J* 6.2 Hz, −CH_2−CH(CH_3)(*C*H_3)); ESI-MS *m*/*z* 341.1 (100 [M + 2Na]$^{2+}$); 658.9 (70 [M + Na]$^+$).

[**11**·2Na]$^{2+}$2TFPB$^-$: ^{1}H NMR (600 MHz, $CDCl_3$) *δ* 7.69 (16H, s, TFPB-*o*-*H*), 7.52 (8H, s, TFPB-*p*-*H*), 7.40 (9H, m, Ar-*m*-*H* and Ar-*p*-*H*), 7.10 (6H, d, *J* 7.1 Hz, Ar-*o*-*H*), 4.79 (3H, d, *J* 16.4 Hz, N−C*H*H-Ph), 4.65 (3H, d, *J* 17.2 Hz, O=C−C*H*H−N−Bn), 4.45 (3H, d, *J* 17.4 Hz, O=C−C*H*H−N-*i*Pr), 4.28 (3H, d, *J* 16.4 Hz, N−CH*H*-Ph), 3.87 (3H, ept, *J* 6.1 Hz, −C*H*(CH_3)$_2$), 3.61 (3H, d, *J* 17.4 Hz, O=C−CH*H*-N-*i*Pr), 3.59 (3H, d, *J* 17.2 Hz, O=C−CH*H*-N-Bn), 1.06 (9H, d, *J* 6.1 Hz, −CH(*C*H_3)(CH_3)), 0.97 (9H, d, *J* 6.1 Hz, −CH(CH_3)(*C*H_3)); ESI-MS *m*/*z* 392.1 (100 [M + 2Na]$^{2+}$); 761.1 (20 [M + Na]$^+$).

[**12**·2Na]$^{2+}$2TFPB$^-$: ^{1}H NMR (600 MHz, $CDCl_3$) *δ* 7.68 (16H, s, TFPB-*o*-*H*), 7.53 (8H, s, TFPB-*p*-*H*), 4.58 (6H, d, *J* 16.7 Hz, O=C−C*H*H−N-*i*Bu), 3.50 (6H, d, *J* 16.7 Hz, O=C−CH*H*-N-*i*Bu), 3.14 (6H, dd, *J* 14.7 and 6.2 Hz, −C*H*H−CH(CH_3)$_2$), 2.94 (6H, dd, *J* 14.7 and 6.5 Hz, −CH*H*−CH(CH_3)$_2$), 1.76 (6H, m, −CH_2−C*H*(CH_3)$_2$), 0.92 (18H, d, *J* 6.0 Hz, −CH_2−CH(*C*H_3)(CH_3)), 0.89 (18H, d, *J* 6.0 Hz, −CH_2−CH(CH_3)(*C*H_3)); ESI-MS *m*/*z* 362.2 (100 [M + 2Na]$^{2+}$); 701.6 (10 [M + Na]$^+$).

[**13**·2Na]$^{2+}$2TFPB$^-$: ^{1}H NMR (600 MHz, $CDCl_3$) *δ* 7.69 (16H, s, TFPB-*o*-*H*), 7.51 (8H, s, TFPB-*p*-*H*), 7.35 (9H, bs, Ar-*m*-*H* and Ar-*p*-*H*), 7.10 (6H, bs, Ar-*o*-*H*), 4.73 (3H, overlapping, br signals, N−C*H*H-Ph), 4.72 (3H, overlapping, br signals, O=C−C*H*H−N−Bn), 4.61 (3H, d, *J* 17.3 Hz, O=C−C*H*H−N-*i*Bu), 4.28 (3H, d, *J* 17.0 Hz, N−CH*H*-Ph), 3.54 (3H, d, *J* 17.3 Hz, O=C−CH*H*-N-*i*Bu), 3.51 (3H, d, *J* 17.0 Hz, N−CH*H*-N-Bn), 3.04 (3H, dd, *J* 14.1 and 6.1 Hz, −C*H*H−CH(CH_3)$_2$), 2.91 (3H, dd, *J* 14.1 and 6.3 Hz, −CH*H*−CH(CH_3)$_2$), 1.69 (3H, m, −CH_2−C*H*(CH_3)$_2$), 0.84 (9H, bs, −CH_2−CH(*C*H_3)-(CH_3)), 0.73 (9H, d, *J* 6.1 Hz, −CH_2−CH(CH_3)(*C*H_3)); ^{13}C NMR (150 MHz, $CDCl_3$) *δ* 169.4 (*C*=O), 168.9 (*C*=O), 161.7 (q, *J* 50 Hz, C-1), 134.8 (C-2), 133.5 (*C*-Ph), 129.6 (*C*H-Ph), 128.7 (q, *J* 30 Hz C-3), 128.5 (*C*H-Ph), 127.3 (*C*H-Ph), 124.6 (q, *J* 270 Hz, C-5), 117.5 (C-4), 56.8 (−CH_2−CH(CH_3)$_2$), 53.1 (*C*H_2-benzyl), 49.3 (O=C-*C*H_2−N), 48.9 (O=C-*C*H_2−N), 27.7 (−CH_2−*C*H(CH_3)$_2$), 19.7 (−CH_3), 19.4 (−CH_3); ESI-MS *m*/*z* 413.5 (100 [M + 2Na]$^{2+}$); 803.0 (20 [M + Na]$^+$).

[**14**·2Na]$^{2+}$2TFPB$^-$: ^{1}H NMR (600 MHz, $CDCl_3$) *δ* 7.72 (16H, s, TFPB-*o*-*H*), 7.52 (8H, s, TFPB-*p*-*H*), 7.30 (18H, m, Ar-*m*-*H* and Ar-*p*-*H*), 6.96 (12H, d, *J* 7.3 Hz, Ar-*o*-*H*), 4.72 (6H, d, *J* 17.2 Hz, O=C−C*H*H−), 4.61 (6H, d, *J* 16.4 Hz, N−C*H*H-Ph), 4.22 (6H, d, *J* 16.4 Hz, N−CH*H*-Ph), 3.57 (6H, d, *J* 17.2 Hz, O=C−CH*H*-); ESI-MS *m*/*z* 464.7 (100 [M + 2Na]$^{2+}$); 906.1 (10 [M + Na]$^+$).

*General Procedure for the Evaluation of the Apparent K_{a1} in [**9**−**14**·Na]$^+$[TFPB]$^-$ and the Apparent K_{a2} in [**13**·2Na]$^{2+}$2[TFPB]$^-$.* To 1.0 mM solutions of cyclic peptoids **9**−**14** in $CHCl_3$ (0.9 mL) was added 1.0 equiv of NaTFPB (previously dissolved in CH_3CN, 0.1 mL). After the addition, the mixtures were sonicated for 5 min in a heated bath (35 °C). The H·G solutions were concentrated under a nitrogen flux and dried under vacuum. The complexes were then dissolved in $CDCl_3$ (1.0 mL) with the help of the sonicator (5−10 min). The H·G complex concentration, at the equilibrium −[H·G]$_{eq}$− was evaluated by integration of the ^{1}H NMR complex signals (2.5−6−0 range) versus the total integration of the free host plus complexed molecules at 298 K. With the addition of 1 equiv of guest, the equilibrium 1 is established (the formation of disodium species is neglected):

$$H + G \rightleftarrows H{\cdot}G \tag{1}$$

Equation 2 was used to obtain the concentration of the [H·G]$_{eq}$ species.

$$[H{\cdot}G]_{eq} = \frac{F_a}{F_b} \times [C]_i \tag{2}$$

where F_a and F_b are the areas of the signals of the host/guest adduct and host plus host/guest adduct, respectively (recorded in the 2.5−6.0 ppm range); $[C]_i$ is the host initial concentration (1.0 mM).

In the case of the formation of a monosodiium complex, the evaluation of the concentration of the species, at the equilibrium, follows the relation 3:

$$[H]_{eq} = [G]_{eq} = [H]_i - [H{\cdot}G]_{eq} \tag{3}$$

The apparent K_{a1} was calculated following eq 4:

$$K_a = \frac{[H{\cdot}G]_{eq}}{[H]_{eq} \times [G]_{eq}} \tag{4}$$

In order to have the reliable integration values, the delay times (D_1) among successive scans, in the ^{1}H NMR, were set at 5 s.

The apparent K_{a2} in [**13**·2Na]$^{2+}$2[TFPB]$^-$ was evaluated in the following way: to 1.0 mM solutions of [**13**·Na]$^+$ in $CDCl_3$ were added proper amounts of NaTFPB (0.2 equiv at a time until 2.0 equiv and then 0.5 equiv until 3.0 equiv). After every addition, the mixture was sonicated for 5 min in a heated bath (35 °C). The ^{1}H NMR spectra were then acquired at 298 K. The apparent K_{a2} was evaluated observing the variation of the chemical shift of the doublet initially at 4.39 ppm, gradually downshifted due to the formation of the bimetallic complex. The data were analyzed by a nonlinear regression analysis using the program WinEQNMR (see Supporting Information).

Computational Methodology. The DFT calculations were performed with the Gaussian09 set of programs,[57] using the BP86 functional of Becke and Perdew.[58] The electronic configuration of the molecular systems (**11**, **11a**, **11b**, [**11**·Na]$^+$, beauvericin (**8**), [**13**·Na]$^+$, [**13**·2Na]$^{2+}$, TFPB$^-$, and NaTFPB; see Supporting Information) was described with the standard triple-ζ valence basis set with a polarization function of Ahlrichs and co-workers for H, B, C, N, O, F, and Na (TZVP keyword in Gaussian).[59] The geometry optimizations were performed without symmetry constraints, and the characterization of the located stationary points was performed by analytical frequency calculations. Solvent effects including contributions of non-electrostatic terms have been estimated in single-point calculations on the gas-phase-optimized structures, based on the polarizable continuous solvation model PCM using $CHCl_3$ as a solvent.[60]

X-ray Crystallography. For compound **9**, colorless needle-like single crystals suitable for X-ray diffraction analysis were obtained by slow evaporation of a solution of chloroform/methanol (1:1) dissolving 2 mg of compound **9** in 1 mL of chloroform. A crystal of 0.43 × 0.20 × 0.15 mm was selected and mounted on a cryoloop with paratone oil and measured at 100 K.

For compound **11**, colorless needle-like single crystals suitable for X-ray diffraction analysis were obtained by diffusion of hexane vapors in a solution obtained dissolving 3 mg of compound **11** in 0.8 mL of chloroform. A crystal of 0.47 × 0.22 × 0.18 mm was selected and mounted on a cryoloop with paratone oil and measured at 100 K.

In both cases, X-ray diffraction measurements were performed with a Rigaku AFC7S diffractometer equipped with a Mercury^2 CCD detector using graphite monochromated Mo Kα radiation (λ = 0.71069 Å). Data reduction was performed with the crystallographic package CrystalClear.[61] Data were corrected for Lorentz, polarization, and absorption.

For the compound **13** as sodium complex, crystals were obtained by slow evaporation of a solution of chloroform/toluene (2:1) dissolving 2 mg of the complex in 1.2 mL of chloroform, followed by addition of 0.6 mL of toluene. A crystal of 0.37 × 0.25 × 0.19 mm was selected and glued on a glass fiber and measured at room temperature by means of a D8QUEST Bruker diffractomenter equipped with PHOTON II detector and IμS 3.0 Microfocus source (Cu Kα radiation).

Data reduction was performed with the crystallographic package APEX3.[62] Data were corrected for Lorentz and polarization effects.

The structures were solved by direct methods using the program SIR2014[63] and refined by means of full matrix least-squares based on F^2 using the program SHELXL.[64] Non-hydrogen atoms were refined anisotropically, and hydrogen atoms were positioned geometrically and included in structure factors calculations but not refined.

For compound **11**, the highest electron density peak in the final difference Fourier map is localized near the second chloroform molecule, which is affected by positional disorder as indicated also by the anisotropic displacement parameters of the chlorine atoms Cl6 and Cl5.

For the sodium complex of **13**, both cubic space groups $Pa\bar{3}$ (no. 205) and $P2_13$ (no. 198) were considered, and final structural refinement was performed in the centrosymmetric one. The presence of the three-fold rotoinversion axis determined the positional disorder of the central cyclopeptoid molecule. This was modeled considering half-occupancy for the benzyl carbon atoms C21, C22, and C23.

Two possible positions were also considered for the isobutyl side chain C4, C5, and C6; these were determined by visual examination of the difference electron density map obtained by omitting the side group by means of the program OLEX2.[65]

For ORTEP and molecular drawings, the program Mercury[66] was used.

CCDC 1544079−1544081 contain the supplementary crystallographic data for this paper. These data are provided free of charge by The Cambridge Crystallographic Data Centre. See Table S2 of the Supporting Information for all the relevant crystallographic data.

Ion Transport Studies. *General Procedures.* L-α-Phosphatidyl-DL-glycerol sodium salt (EYPG, 20 mg/mL chloroform solution) was purchased from Avanti Polar Lipids; egg yolk phosphatidylcholine (EYPC, 100 mg/mL chloroform solution), cholesterol, and 8-hydroxypyrene-1,3,6-trisulfonic acid trisodium salt (HPTS) were from Sigma; Triton X-100 and HEPES buffer were from Fluka; all salts were of the best grade available from Aldrich and were used without further purification. Liposomes were prepared by extrusion using a 10 mL LipexTM Thermobarrel EXTRUDER (Northern Lipids Inc.) connected to a thermostatic bath kept at 25 °C. The 100 nm polycarbonate membranes were nucleopore track-etch membranes from Whatman. Fluorescence spectra were recorded on a Varian Cary Eclipse fluorescence spectrophotometer. All fluorimetric measurements were performed at 25 °C. The ionophore concentration is given in percent with respect to the total concentration of lipids. Mother solutions of ionophores were prepared in DMSO. Control experiments showed that the amount of DMSO added to the vesicular suspension in the different experiments (maximum amount 8% in volume) did not affect the permeability of the membrane.

HPTS Assay. A mixture of 150 μL of EYPC chloroform solution (100 mg/mL, 20 μmol) and 40 μL of EYPG chloroform solution (20 mg/mL, 1 μmol) was first evaporated under Ar flux to form a thin film and then dried under high vacuum for 3 h. If required, further 70 μL of cholesterol chloroform solution was added (50 mg/mL, 9 μmol). The lipid cake was hydrated in 1.5 mL of 0.1 mM HPTS solution (HEPES 25 mM, 100 mM NaCl, pH 7) for 30 min at 40 °C. The lipid suspension was submitted to 5 freeze−thaw cycles (−196 °C/40 °C) using liquid nitrogen and a thermostatic bath and then extruded under nitrogen pressure (15 bar) at room temperature (10 extrusions through a 0.1 μm polycarbonate membrane). The LUV suspension was separated from extravesicular dye by size exclusion chromatography (stationary phase: prepacked column Sephadex G-25, mobile phase: HEPES buffer 25 mM, 100 mM NaCl, pH 7) and diluted with HEPES buffer (HEPES 25 mM, 100 mM NaCl, pH 7) to give a stock solution with a lipid concentration of 5 mM (assuming 100% of lipids were incorporated into liposomes). Next, 104 μL of the lipid suspension was placed in a fluorimetric cell and diluted to 3040 μL with the appropriate buffer solution (25 mM HEPES, pH 7) containing 100 mM of the salt under investigation (MCl with M = Li^+, Na^+, K^+, Rb^+, Cs^+; NaX with X = Cl^-, Br^-, I^-, 50 mM in the case of $CaCl_2$). The total lipid concentration in the fluorimetric cell was 0.17 mM. An aliquot of solution of the ionophore in DMSO (10−80 μL of the appropriate mother solution in order to obtain the desired $mol_{compound}/mol_{lipid}$ ratio) was then added to the lipid suspension, and the cell was incubated at 25 °C for 10 min. After incubation, the time course of fluorescence was recorded for 50 s monitoring the HPTS emission at 510 nm with excitation wavelengths set alternatively at 403 and 460 nm on a 0.5 + 0.5 s cycle. Then 50 μL of 0.5 M MOH (with M = Li^+, Na^+, K^+, Rb^+, Cs^+, depending on the cation present in the extravesicular solution) was rapidly added through an injector port, and the fluorescence emission was recorded for 300 s. In the case of the experiment with the protonophore, the solution of MOH was added first, and then, after 25 s, a DMSO solution of CCCP was added (5 μL) in order to get a concentration of 5%. The fluorescence was monitored for a further 40 s in order to verify the impermeability of the liposomes, and then an aliquot of DMSO solution of the ionophore was added and the fluorescence was monitored for 260 s. In each experiment, maximal changes in dye emission were obtained by final lysis of the liposomes with a detergent (40 μL of 5% aqueous Triton X-100). The data set consists of emission intensities at 510 nm modulated by alternating excitation at 403 and 460 nm on a 0.5 + 0.5 s cycle. The concentration of the conjugate base form of HPTS is related to the emission intensity at 510 nm during the period in which the dye is excited at 460 nm (E_{460}), whereas the concentration of the protonated form is related to the emission intensity at 510 nm during the period in which the dye is excited at 403 nm (E_{403}). Fluorescence time courses were normalized using the following equation, where the subscripts 0, ∞, and t denote the emission ratio before the base pulse, after detergent lysis, and at an intermediate time, respectively.

$$\mathrm{Fl} = \frac{\left(\frac{E_{403}}{E_{460}}\right)_t - \left(\frac{E_{403}}{E_{460}}\right)_0}{\left(\frac{E_{403}}{E_{460}}\right)_\infty - \left(\frac{E_{403}}{E_{460}}\right)_0} \times 100$$

Cytotoxic Activities. *Cell Viability Assay.* A375 human melanoma cells and PC3 (PC-3) human prostate cancer cell lines (American Type Culture Collection, Manassa, VA) were used. Cells were cultured in Dulbecco's modified Eagle or RPMI 1640 medium, supplemented with 10% (v/v) FBS, 2 mM L-glutamine and antibiotics (100 U/mL penicillin, 100 μg/mL streptomycin) at 37 °C in humidified atmosphere with 5% CO_2. To ensure logarithmic growth, cells were subcultured every 2 days. A375 and PC-3 cells were seeded in triplicate in 96-well plates (3000/well) and incubated for the 72 h in the absence or presence of different concentrations (2−50 μM) of cyclic peptoids **9**−**14** or linear peptoids **15**−**19**. Stock solutions of compounds (25 mM in DMSO) were stored at −20 °C and diluted just before addition to the sterile culture medium. Beauvericin, purchased from (Santa Cruz Biotechnology, Inc., Delaware, CA, USA), was used in the same experimental condition at a concentration ranging from 0.5 to 5 μM. In all the experiments, final concentration of DMSO was 0.2% (v/v). The number of viable cells was determined by using a [3-4,5-dimethyldiazol-2-yl]-2,5-diphenyl tetrazolium bromide (MTT, Sigma-Aldrich) conversion assay, as previously described.[67] IC_{50} values were calculated from cell viability dose−response curves and defined as the concentration resulting in 50% inhibition of cell survival, compared to control cells treated with DMSO.

Cell Cycle Distribution Analysis. Cell DNA content was measured by propidium iodide (PI) incorporation into permeabilized cells, as described by Nicoletti et al.[68] Briefly, the cells were harvested after treatment with compounds washed with cold PBS and incubated with a PI solution (0.1% sodium citrate, 0.1% Triton X-100 and 25 μg/mL of prodium iodide, Sigma-Aldrich, 10 μg/mL RNase A) for 30 min at 4 °C. Data from 10000 events for each sample were collected by a FACScalibur flow cytometry (Becton Dickinson, San Jose, CA), and cellular debris was excluded from analysis by raising the forward scatter threshold. Percentage of cells in the sub-G_0/G_1 phase, hypodiploid region, was quantified using the CellQuest software (Becton Dickinson). The distribution of cells in G_0/G_1, S, and G_2/M phases was determined using ModFit LT cell cycle analysis software (Becton Dickinson).

Statistical Analysis. All reported data represent the mean ± SD of at least three independent experiments performed in triplicate. The statistical significance of cell cycle distribution results was performed by the two-way analysis of variance with Bonferroni post-test analysis using GraphPad Prism 5 software. The P value $\leq$0.05 was considered significant.

■ ASSOCIATED CONTENT

Supporting Information

The Supporting Information is available free of charge on the ACS Publications website at DOI: 10.1021/acs.joc.7b00965.

X-ray data for compound **9** (CIF)
X-ray data for compound **11** (CIF)
X-ray data for compound **13** (CIF)
1D and 2D spectra of cyclic peptoids and their complexes, ^{1}H NMR variable temperature and titration experiments, ESI-MS spectra, HPLC chromatograms of linear and cyclic peptoids, minimum energy structures and Cartesian coordinates, ionophoric assays, and X-ray data (PDF)

■ AUTHOR INFORMATION

Corresponding Authors

*E-mail: iizzo@unisa.it.
*E-mail: dericca@unisa.it.

ORCID

Giorgio Della Sala: 0000-0001-5020-8502
Irene Izzo: 0000-0002-0369-0102
Francesco De Riccardis: 0000-0002-8121-9463

Notes

The authors declare no competing financial interest.

■ ACKNOWLEDGMENTS

Financial support from the University of Salerno (FARB), the Italian Ministero dell'Università e della Ricerca (MIUR) (PRIN 20109Z2XRJ_006), Regione Campania under POR Campania "FESR 2007-2013-O.O. 2.1 (FarmaBioNet)" and from POR CAMPANIA FESR 2007/2013 O.O.2.1.-CUP B46D14002660009 "Il potenziamento e la riqualificazione del sistema delle infrastrutture nel settore dell'istruzione, della formazione e della ricerca". We thank Dr. Patrizia Iannece for HR-ESI-MS. We also thank Dr. Carmen Talotta (University of Salerno) for valuable discussion and gift of NaTFPB, and Dr. Rosaria Schettini (University of Salerno) for the gift of **14**.

■ REFERENCES

(1) Clardy, J.; Walsh, C. *Nature* **2004**, *432*, 829−837.
(2) Wender, P. A.; Miller, B. L. *Nature* **2009**, *460*, 197−201.
(3) (a) Sun, J.; Zuckermann, R. N. *ACS Nano* **2013**, *7*, 4715−4732. (b) Zhang, D.; Lahasky, S. H.; Guo, L.; Lee, C. U.; Lavan, M. *Macromolecules* **2012**, *45*, 5833−5841. (c) Zuckermann, R. N. *Biopolymers* **2011**, *96*, 545−555. (d) Yoo, B.; Shin, S. B. Y.; Huang, M. L.; Kirshenbaum, K. *Chem. - Eur. J.* **2010**, *16*, 5528−5537. (e) Zuckermann, R. N.; Kodadek, T. *Curr. Opin. Mol. Ther.* **2009**, *11*, 299−307. (f) Fowler, S. A.; Blackwell, H. E. *Org. Biomol. Chem.* **2009**, *7*, 1508−1524. (g) Yoo, B.; Kirshenbaum, K. *Curr. Opin. Chem. Biol.* **2008**, *12*, 714−721.
(4) (a) Meli, A.; Gambaro, S.; Costabile, C.; Talotta, C.; Della Sala, G.; Tecilla, P.; Milano, D.; Tosolini, M.; Izzo, I.; De Riccardis, F. *Org. Biomol. Chem.* **2016**, *14*, 9055−9062. (b) Izzo, I.; Ianniello, G.; De Cola, C.; Nardone, B.; Erra, L.; Vaughan, G.; Tedesco, C.; De Riccardis, F. *Org. Lett.* **2013**, *15*, 598−601. (c) Lepage, M. L.; Meli, A.; Bodlenner, A.; Tarnus, C.; De Riccardis, F.; Izzo, I.; Compain, P. *Beilstein J. Org. Chem.* **2014**, *10*, 1406−1412. (d) De Cola, C.; Licen, S.; Comegna, D.; Cafaro, E.; Bifulco, G.; Izzo, I.; Tecilla, P.; De Riccardis, F. *Org. Biomol. Chem.* **2009**, *7*, 2851−2854. (e) Maulucci, N.; Izzo, I.; Bifulco, G.; Aliberti, A.; De Cola, C.; Comegna, D.; Gaeta, C.; Napolitano, A.; Pizza, C.; Tedesco, C.; Flot, D.; De Riccardis, F. *Chem. Commun.* **2008**, 3927−3929.
(5) (a) Spandl, R. J.; Bender, A.; Spring, D. R. *Org. Biomol. Chem.* **2008**, *6*, 1149−1158. (b) Lehn, J.-M. *Proc. Natl. Acad. Sci. U. S. A.* **2002**, *99*, 4763−4768.
(6) (a) Bills, G.; Li, Y.; Chen, L.; Yue, Q.; Niu, X.-M.; An, Z. *Nat. Prod. Rep.* **2014**, *31*, 1348−1375. (b) Sivanathan, S.; Scherkenbeck, J. *Molecules* **2014**, *19*, 12368−12420. (c) Sy-Cordero, A. A.; Pearce, C. J.; Oberlies, N. H. *J. Antibiot.* **2012**, *65*, 541−549. (d) Wang, Q.; Xu, L. *Molecules* **2012**, *17*, 2367−2377. (e) Süssmuth, R.; Müller, J.; Von Döhren, H.; Molnár, I. *Nat. Prod. Rep.* **2011**, *28*, 99−124.
(7) (a) Dodziuk, H. *Tetrahedron: Asymmetry* **1992**, *3*, 43−50. (b) McIldowie, M. J.; Mocerino, M.; Ogden, M. I. *Supramol. Chem.* **2010**, *22*, 13−39. (c) Testa, B. *Helv. Chim. Acta* **2013**, *96*, 351−372. (d) Eliel, E. L.; Wilen, S. H.; Mander, L. N. *Stereochemistry of Organic Compounds*; John Wiley & Sons, 1994; pp 1119−1190. (e) Cahn, R. S.; Ingold, C.; Prelog, V. *Angew. Chem., Int. Ed. Engl.* **1966**, *5*, 385−415. (f) Prelog, V.; Helmchen, G. *Angew. Chem., Int. Ed. Engl.* **1982**, *21*, 567−583.
(8) (a) Kaminsky, R.; Ducray, P.; Jung, M.; Clover, R.; Rufener, L.; Bouvier, J.; Weber, S. S.; Wenger, A.; Wieland-Berghausen, S.; Goebel, T.; et al. *Nature* **2008**, *452*, 176−180. (b) Endo, M.; Takesako, K.; Kato, I.; Yamaguchi, H. *Antimicrob. Agents Chemother.* **1997**, *41*, 672−676.
(9) Chatterjee, J.; Rechenmacher, F.; Kessler, K. *Angew. Chem., Int. Ed.* **2013**, *52*, 254−269.
(10) (a) Ovchinnikov, Y. A.; Ivanov, V. T.; Evstratov, A. V.; Mikhaleva, I. I.; Bystrov, V. F.; Portnova, S. L.; Balashova, T. A.; Meshcheryakova, E. N.; Tulchinsky, V. M. *Int. J. Pept. Protein Res.* **1974**, *6*, 465−498. (b) Cuomo, V.; Randazzo, A.; Meca, G.; Moretti, A.; Cascone, A.; Eriksson, O.; Novellino, E.; Ritieni, A. *Food Chem.* **2013**, *140*, 784−793.
(11) (a) Makrlík, E.; Böhm, S.; Vaňura, P. *Monatsh. Chem.* **2016**, *147*, 1687−1692. (b) Makrlík, E.; Böhm, S.; Vaňura, P.; Raich, I. *J. Mol. Struct.*

2014, *1076*, 564−567. (c) Makrlík, E.; Toman, P.; Vaňura, P. *Acta Chim. Slov.* **2013**, *60*, 884−888.
(12) The ionophoric activities of enniatins has been known since the 1960s: (a) Shemyakin, M. M.; Ovchinnikov, Y. A.; Ivanov, V. T.; Antonov, V. K.; Vinogradova, E. I.; Shkrob, A. M.; Malenkov, G. G.; Evstratov, A. V.; Laine, I. A.; Melnik, E. I.; Ryabova, I. D. *J. Membr. Biol.* **1969**, *1*, 402−430. (b) Kamyar, M.; Rawnduzi, P.; Studenik, C. R.; Kouri, K.; Lemmens-Gruber, R. *Arch. Biochem. Biophys.* **2004**, *429*, 215−223.
(13) Comegna, D.; Benincasa, M.; Gennaro, R.; Izzo, I.; De Riccardis, F. *Bioorg. Med. Chem.* **2010**, *18*, 2010−2018.
(14) Previous contributions showed that in cyclodepsipeptides it is possible to substitute the ester junction with a methyl amide with no major effects on the biological activity. See: Izzo, I.; Acosta, G. A.; Tulla-Puche, J.; Cupido, T.; Martin-Lopez, M. J.; Cuevas, C.; Albericio, F. *Eur. J. Org. Chem.* **2010**, 2536−2543. The advantage of this substitution is represented by the higher stability of the amide bond and the easier solid-phase synthesis of the corresponding linear oligoamides.
(15) The translation of a peptide chain in a linear peptoid chain can afford peptoid or retro-peptoid peptidomimetics: Kruijtzer, J. A.W.; Liskamp, R. M. J. *Tetrahedron Lett.* **1995**, *36*, 6969−6972. In the case of cyclic peptoids (with no C- or N-termini), there is no formal difference.
(16) (a) De Riccardis, F.; Izzo, I.; Montesarchio, D.; Tecilla, P. *Acc. Chem. Res.* **2013**, *46*, 2781−2790. (b) Montenegro, J.; Ghadiri, M. R.; Granja, J. R. *Acc. Chem. Res.* **2013**, *46*, 2955−2965.
(17) There is a vast literature on the antitumor potential of *linear* peptoids. Udugamasooriya, G. *Biomol. Res. Ther.* **2014**, *3*, 1−3 and references cited therein.
(18) (a) Zuckermann, R. N.; Kerr, J. M.; Kent, S. B. H.; Moos, W. H. *J. Am. Chem. Soc.* **1992**, *114*, 10646−10647. (b) Della Sala, G.; Nardone, B.; De Riccardis, F.; Izzo, I. *Org. Biomol. Chem.* **2013**, *11*, 726−731.
(19) De Cola, C.; Fiorillo, G.; Meli, A.; Aime, S.; Gianolio, E.; Izzo, I.; De Riccardis, F. *Org. Biomol. Chem.* **2014**, *12*, 424−431.
(20) ^{1}H NMR spectra run in different deuterated solvents or mixtures—pyridine-d_6, benzene-d_6, $CD_3CN/CDCl_3$ (9:1)—did not improve the isomers ratio. It is interesting to note that benzyl groups can stabilize *cis*-peptoid junction for the well-studied n→π* interaction between the carbonyl lone pairs and the aromatic π * orbitals. See: (a) Gorske, B. C.; Bastian, B. L.; Geske, G. D.; Blackwell, H. E. *J. Am. Chem. Soc.* **2007**, *129*, 8928−8929. **11** is the first case of a conformationally stable non-N-arylated hexameric cyclic peptoid. It must be noted that the conformational heterogeneity evident in the NMR spectra of the 18-membered cyclic peptoids is known since the late 1960s; see: (b) Dale, J.; Titlestad, K. *J. Chem. Soc. D* **1969**, 656−659.
(21) The first NMR structure of a conformationally stable cyclic peptoid was reported for a *cttct* bis-N-arylated hexamer: (a) Shah, N. H.; Butterfoss, G. L.; Nguyen, K.; Yoo, B.; Bonneau, R.; Rabenstein, D. L.; Kirshenbaum, K. *J. Am. Chem. Soc.* **2008**, *130*, 16622−16632. For the NMR assignment of conformationally stable cyclic octameric peptoids, see: (b) Vollrath, S. B. L.; Hu, C.; Bräse, S.; Kirshenbaum, K. *Chem. Commun.* **2013**, *49*, 2317−2319. (c) Vollrath, S. B. L.; Bräse, S.; Kirshenbaum, K. *Chem. Sci.* **2012**, *3*, 2726−2731. For the NMR assignment of conformationally stable smaller cyclic peptoids, see: Culf, A. S.; Čuperlović-Culf, M.; Léger, D. A.; Decken, A. *Org. Lett.* **2014**, *16*, 2780−2783 and ref 20b.
(22) (a) De Santis, E.; Edwards, A. A.; Alexander, B. D.; Holder, S. J.; Biesse-Martin, A. S.; Nielsen, B. V.; Mistry, D.; Waters, L.; Siligardi, G.; Hussain, R.; Faure, S.; Taillefumier, C. *Org. Biomol. Chem.* **2016**, *14*, 11371−11380. (b) Armand, P.; Kirshenbaum, K.; Goldsmith, R. A.; Farr-Jones, S.; Barron, A. E.; Truong, K. T. V.; Dill, K. A.; Mierke, D. F.; Cohen, F. E.; Zuckermann, R. N.; Bradley, E. K. *Proc. Natl. Acad. Sci. U. S. A.* **1998**, *95*, 4309−4314.
(23) The *cctcct* arrangement is the favorite peptide bond geometry sequence for most of the solid-state hexameric cyclic peptoid structures reported. In the case of complexed hexameric cyclopeptoids all-*trans* peptoid junctions are observed: Tedesco, C.; Erra, L.; Izzo, I.; De Riccardis, F. *CrystEngComm* **2014**, *16*, 3667−3687.
(24) Variable temperature ^{1}H NMR experiments showed for cyclo-[*cctcct*]-**11** a coalescence temperature (T_c) at 323 K (in $C_2D_2Cl_4$ solution, 300 MHz, $\Delta G^{\ddagger}$ = 14.4 kcal mol^{-1}); the value was calculated according to Kurland, R. J.; Rubin, M. B.; Wise, M. B. *J. Chem. Phys.* **1964**, *40*, 2426−2427.
(25) Groth, P. *Acta Chem. Scand. A* **1977**, *31*, 838−840.
(26) Shin, S. B. Y.; Yoo, B.; Todaro, L. J.; Kirshenbaum, K. *J. Am. Chem. Soc.* **2007**, *129*, 3218−3225.
(27) Geddes, A. J.; Akrigg, D. *Acta Crystallogr., Sect. B: Struct. Crystallogr. Cryst. Chem.* **1976**, *32*, 3164−3171.
(28) Beauvericin (**8**) was modeled according to DFT studies (see Experimental Section).
(29) (a) Baskin, M.; Panz, L.; Maayan, G. *Chem. Commun.* **2016**, *52*, 10350−10353. (b) Baskin, M.; Maayan, G. *Chem. Sci.* **2016**, *7*, 2809−2820. (c) Knight, A. S.; Zhou, E. Y.; Francis, M. B. *Chem. Sci.* **2015**, *6*, 4042−4048. (d) Baskin, M.; Maayan, G. *Biopolymers* **2015**, *104*, 577−584. (e) *Metallofoldamers. Supramolecular Architectures from Helicates to Biomimetics* Maayan, G., Albrecht, M., Eds.; John Wiley & Sons, 2013. (f) Knight, A. S.; Zhou, E. Y.; Pelton, J. G.; Francis, M. B. *J. Am. Chem. Soc.* **2013**, *135*, 17488−17493. (g) Maayan, G.; Ward, M. D.; Kirshenbaum, K. *Chem. Commun.* **2009**, 56−58. (h) Maayan, G. *Eur. J. Org. Chem.* **2009**, 5699−5710. (i) Lee, B. C.; Chu, T. K.; Dill, K. A.; Zuckermann, R. N. *J. Am. Chem. Soc.* **2008**, *130*, 8847−8855.
(30) It is known that, for similar sodium complexed hexameric cyclic peptoids, there is no glimpse of coalescence (conformational inversion) at temperatures >150 °C for the strong carbonyl/metal additive ione−dipole interactions. See reference 4e.
(31) From: (a) Singh, M. D.; Siegel, J.; Biali, S. E.; Mislow, K. *J. Am. Chem. Soc.* **1987**, *109*, 3397−3402. See also: (b) Prelog, V.; Gerlach, H. *Helv. Chim. Acta* **1964**, *47*, 2288−2294. (c) Goodman, M.; Chorev, M. *Acc. Chem. Res.* **1979**, *12*, 1−7.
(32) From: Dalla Cort, A.; Mandolini, L.; Pasquini, C.; Schiaffino, L. *New J. Chem.* **2004**, *28*, 1198−1199.
(33) (a) Reuter, C.; Schmieder, R.; Vögtle, F. *Pure Appl. Chem.* **2000**, *72*, 2233−2241. (b) Mislow, K. *Croat. Chem. Acta* **1996**, *69*, 485−511.
(34) (a) Szumna, A. *Org. Biomol. Chem.* **2007**, *5*, 1358−1368. (b) Szumna, A. *Chem. Soc. Rev.* **2010**, *39*, 4274−4285.
(35) Metal complexes of cyclic peptoids with identical side chains and all-*trans* peptoid bond geometry (like the sodium salt expected to be formed from **9**, **12**, and **14**) are achiral for the presence of a S_6 symmetry axis. See reference 4e.
(36) (a) Shemyakin, M. M.; Ovchinnikov, Yu. A.; Ivanov, V. T.; Evstratov, A. V. *Nature* **1967**, *213*, 412−413. (b) Shemyakin, M. M.; Ovchinnikov, Yu. A.; Ivanov, V. T. *Angew. Chem., Int. Ed. Engl.* **1969**, *8*, 492−499.
(37) (a) Juvvadi, P.; Vunnam, S.; Merrifield, R. B. *J. Am. Chem. Soc.* **1996**, *118*, 8989−8997. (b) Vunnam, S.; Juvvadi, P.; Rotondi, K. S.; Merrifield, R. B. *J. Pept. Res.* **1998**, *51*, 38−44.
(38) For the binding studies, we chose the sodium cation for its high affinity toward the hexameric cyclic peptoids (see references 4d and 4e) and for the sodium ion relevance in biological systems.
(39) Nishida, H.; Takada, N.; Yoshimura, M.; Sonoda, T.; Kobayashi, H. *Bull. Chem. Soc. Jpn.* **1984**, *57*, 2600−2604.
(40) (a) Schettini, R.; Nardone, B.; De Riccardis, F.; Della Sala, G.; Izzo, I. *Eur. J. Org. Chem.* **2014**, 7793−7797.
(41) (a) Fielding, L. *Tetrahedron* **2000**, *56*, 6151−6170. The term "apparent" is due to the low solubility of the guest in $CDCl_3$. See: (b) Bright, A. A. S.; Chudek, J. A.; Foster, R. *J. Chem. Soc., Perkin Trans. 2* **1975**, *109*, 1256−1259. (c) Talotta, C.; Gaeta, C.; Neri, P. *J. Org. Chem.* **2014**, *79*, 9842−9846.
(42) For recent examples of inverse sandwich, see: Edelmann, F. T. *Coord. Chem. Rev.* **2017**, *338*, 27−140.
(43) Because of the gradual formation of a precipitate in the NMR sample, it was possible to fully characterize (^{1}H and ^{13}C NMR) just the most soluble cyclopeptoid [**13**·2Na]$^{2+}$ complex (see Supporting Information). The use of more polar/coordinating solvents, like CD_3CN (in order to increase the solubility of the complexes), disrupts the dimetal hosts/guest adducts (for the exalted coordination abilities of donor atoms) and re-establishes the 1:1 complexes. The formation of the bimetallic species in presence of an excess of NaTFPB guest in $CDCl_3$ has been previously observed. See reference 4a.

(44) The crystallographic three-fold rotation axis determines the positional disorder of benzyl and isobutyl moieties in the central cyclopeptoid molecule.
(45) Braden, B.; Hamilton, J. A.; Sabesan, M. N.; Steinrauf, L. K. *J. Am. Chem. Soc.* **1980**, *102*, 2704−2709.
(46) Berezin, S. K. *J. Membr. Biol.* **2015**, *248*, 713−726.
(47) Sakai, N.; Matile, S. *J. Phys. Org. Chem.* **2006**, *19*, 452−460.
(48) Wu, X.; Judd, L. W.; Howe, E. N. W.; Withecombe, A. M.; Soto-Cerrato, V.; Li, H.; Busschaert, N.; Valkenier, H.; Pérez-Tomás, R.; Sheppard, D. N.; Jiang, Y.-B.; Davis, A. P.; Gale, P. A. *Chem.* **2016**, *1*, 127−146.
(49) Knight, N. J.; Hernando, E.; Haynes, C. J. E.; Busschaert, N.; Clarke, H. J.; Takimoto, K.; García-Valverde, M.; Frey, J. G.; Quesada, R.; Gale, P. A. *Chem. Sci.* **2016**, *7*, 1600−1608.
(50) Adriaenssens, L.; Estarellas, C.; Jentzsch, A. V.; Belmonte, M. M.; Matile, S.; Ballester, P. *J. Am. Chem. Soc.* **2013**, *135*, 8324−8330.
(51) (a) Moore, S. J.; Haynes, C. J. E.; Gonzalez, J.; Sutton, J. L.; Brooks, S. J.; Light, M. E.; Herniman, J.; Langley, G. J.; Soto-Cerrato, V.; Pérez-Tomás, R.; Marques, I.; Costa, P. J.; Félix, V.; Gale, P. A. *Chem. Sci.* **2013**, *4*, 103−117. (b) Busschaert, N.; Karagiannidis, L. E.; Wenzel, M.; Haynes, C. J. E.; Wells, N. J.; Young, P. G.; Makuc, D.; Plavec, J.; Jolliffe, K. A.; Gale, P. A. *Chem. Sci.* **2014**, *5*, 1118−1127.
(52) Tonshin, A. A.; Teplova, V. V.; Andersson, M. A.; Salkinoja-Salonen, M. S. *Toxicology* **2010**, *276*, 49−57.
(53) Zhan, J.; Burns, A. M.; Liu, M. X.; Faeth, S. H.; Gunatilaka, A. A. *J. Nat. Prod.* **2007**, *70*, 227−232.
(54) Dornetshuber, R.; Heffeter, P.; Lemmens-Gruber, R.; Elbling, L.; Marko, D.; Micksche, M.; Berger, W. *Mol. Nutr. Food Res.* **2009**, *53*, 1112−1122.
(55) Prosperini, A.; Juan-García, A.; Font, G.; Ruiz, M. J. *Toxicol. Lett.* **2013**, *222*, 36−44.
(56) Lu, C. L.; Lin, H. I.; Chen, B. F.; Jow, G. M. *J. Toxicol. Sci.* **2016**, *41*, 429−437.
(57) Frisch, M. J.; Trucks, G. W.; Schlegel, H. B.; Scuseria, G. E.; Robb, M. A.; Cheeseman, J. R.; Scalmani, G.; Barone, V.; Mennucci, B.; Petersson, G. A.; Nakatsuji, H.; Caricato, M.; Li, X.; Hratchian, H. P.; Izmaylov, A. F.; Bloino, J.; Zheng, G.; Sonnenberg, J. L.; Hada, M.; Ehara, M.; Toyota, K.; Fukuda, R.; Hasegawa, J.; Ishida, M.; Nakajima, T.; Honda, Y.; Kitao, O.; Nakai, H.; Vreven, T.; Montgomery, J. A., Jr.; Peralta, J. E.; Ogliaro, F.; Bearpark, M.; Heyd, J. J.; Brothers, E.; N. Kudin, K.; Staroverov, V. N.; Kobayashi, R.; Normand, J.; Raghavachari, K.; Rendell, A.; Burant, J. C.; Iyengar, S. S.; Tomasi, J.; Cossi, M.; Rega, N.; Millam, J. M.; Klene, M.; Knox, J. E.; Cross, J. B.; Bakken, V.; Adamo, C.; Jaramillo, J.; Gomperts, R.; Stratmann, R. E.; Yazyev, O.; Austin, A. J.; Cammi, R.; Pomelli, C.; Ochterski, J. W.; Martin, R. L.; Morokuma, K.; Zakrzewski, V. G.; Voth, G. A.; Salvador, P.; Dannenberg, J. J.; Dapprich, S.; Daniels, A. D.; Farkas, O.; Foresman, J. B.; Ortiz, J. V.; Cioslowski, J.; Fox, D. J.*Gaussian 09*, revision A.02; Gaussian, Inc.: Wallingford, CT, 2009.
(58) (a) Becke, A. *Phys. Rev. A: At., Mol., Opt. Phys.* **1988**, *38*, 3098−3100. (b) Perdew, J. P. *Phys. Rev. B: Condens. Matter Mater. Phys.* **1986**, *33*, 8822−8824. (c) Perdew, J. P. *Phys. Rev. B: Condens. Matter Mater. Phys.* **1986**, *34*, 7406−7406.
(59) Schaefer, A.; Huber, C.; Ahlrichs, R. *J. Chem. Phys.* **1994**, *100*, 5829−5835.
(60) (a) Barone, V.; Cossi, M. *J. Phys. Chem. A* **1998**, *102*, 1995−2001. (b) Tomasi, J.; Persico, M. *Chem. Rev.* **1994**, *94*, 2027−2094.
(61) *CrystalClear*, Crystal Structure Analysis Package; Rigaku-Molecular Structure Corp.
(62) *APEX3*. Bruker AXS Inc.: Madison, Wisconsin, USA.
(63) Burla, M. C.; Caliandro, R.; Carrozzini, B.; Cascarano, G. L.; Cuocci, C.; Giacovazzo, C.; Mallamo, M.; Mazzone, A.; Polidori, G. *J. Appl. Crystallogr.* **2015**, *48*, 306−309.
(64) Sheldrick, G. M. *Acta Crystallogr., Sect. C: Struct. Chem.* **2015**, *71*, 3−8.
(65) Dolomanov, O. V.; Bourhis, L. J.; Gildea, R. J.; Howard, J. A. K.; Puschmann, H. *J. Appl. Crystallogr.* **2009**, *42*, 339−341.
(66) Macrae, C. F.; Bruno, I. J.; Chisholm, J. A.; Edgington, P. R.; McCabe, P.; Pidcock, E.; Rodriguez-Monge, L.; Taylor, R.; van de Streek, J.; Wood, P. A. *J. Appl. Crystallogr.* **2008**, *41*, 466−470.
(67) Terracciano, S.; Chini, M. G.; Vaccaro, M. C.; Strocchia, M.; Foglia, A.; Vassallo, A.; Saturnino, C.; Riccio, R.; Bifulco, G.; Bruno, I. *Chem. Commun.* **2016**, *52*, 12857−12860.
(68) Nicoletti, I.; Migliorati, G.; Pagliacci, M. C.; Grignani, F.; Riccardi, C. *J. Immunol. Methods* **1991**, *139*, 271−279.